AGU ADVANCING EARTH AND SPACE SCIENCES

Water Resources Research

RESEARCH ARTICLE
10.1029/2023WR035044

Local Topography and Streambed Hydraulic Conductivity Influence Riparian Groundwater Age and Groundwater-Surface Water Connection

S. R. Warix[1], A. Navarre-Sitchler[1], A. H. Manning[2], and K. Singha[1]

[1]Hydrologic Science and Engineering Program, Colorado School of Mines, Golden, CO, USA, [2]United States Geological Survey, Denver, CO, USA

Key Points:

- Mean groundwater age is youngest in areas with high slope and streambed hydraulic conductivity
- Mean groundwater age shifts older during low flow periods
- Future stream drying is more probable where local slope and streambed hydraulic conductivity are high

Supporting Information:

Supporting Information may be found in the online version of this article.

Correspondence to:

S. R. Warix,
swarix@mines.edu

Citation:

Warix, S. R., Navarre-Sitchler, A., Manning, A. H., & Singha, K. (2023). Local topography and streambed hydraulic conductivity influence riparian groundwater age and groundwater-surface water connection. *Water Resources Research*, *59*, e2023WR035044. https://doi.org/10.1029/2023WR035044

Received 1 MAY 2023
Accepted 22 AUG 2023

Author Contributions:

Conceptualization: S. R. Warix, A. Navarre-Sitchler, K. Singha
Data curation: S. R. Warix
Formal analysis: S. R. Warix
Funding acquisition: A. Navarre-Sitchler, K. Singha
Methodology: S. R. Warix, A. Navarre-Sitchler, A. H. Manning, K. Singha
Project Administration: A. Navarre-Sitchler, K. Singha
Supervision: A. Navarre-Sitchler, K. Singha
Visualization: S. R. Warix
Writing – original draft: S. R. Warix
Writing – review & editing: S. R. Warix, A. Navarre-Sitchler, A. H. Manning, K. Singha

Abstract The western U.S. is experiencing increasing rain to snow ratios due to climate change, and scientists are uncertain how changing recharge patterns will affect future groundwater-surface water connection. We examined how watershed topography and streambed hydraulic conductivity impact groundwater age and stream discharge at eight sites along a headwater stream within the Manitou Experimental Forest, CO USA. To do so, we measured: (a) continuous stream and groundwater discharge/level and specific conductivity from April to November 2021; (b) biweekly stream and groundwater chemistry; (c) groundwater chlorofluorocarbons and tritium in spring and fall; (d) streambed hydraulic conductivity; and (e) local slope. We used the chemistry data to calculate fluorite saturation states that were used to inform end-member mixing analysis of streamflow source. We then combined chlorofluorocarbon and tritium data to estimate the age composition of riparian groundwater. Our data suggest that future stream drying is more probable where local slope is steep and streambed hydraulic conductivity is high. In these areas, groundwater source shifted seasonally, as indicated by age increases, and we observed a high fraction of groundwater in streamflow, primarily interflow from adjacent hillslopes. In contrast, where local slope is flat and streambed hydraulic conductivity is low, streamflow is more likely to persist as groundwater age was seasonally constant and buffered by storage in alluvial sediments. Groundwater age and streamflow paired with characterization of watershed topography and subsurface characteristics enabled identification of likely controls on future stream drying patterns.

Plain Language Summary In the western U.S., climate change is causing more precipitation to fall as rain rather than snow and it is currently unclear how, where, and when this shift is going to impact groundwater contributions to streams, which is important for predicting streamflow and many ecosystem services, including stream contaminant processing or thermal refugia for fish habitat. In this study, we instrumented a small, high-elevation stream in Colorado, USA to determine (a) how much groundwater is contributing to streamflow and (b) how long groundwater spends traveling through the subsurface before doing so. We found that groundwater age ranged from 10 to 55 years, with older groundwater located in areas with flat topography and where water could not move through streambed sediment quickly. We found the areas with steeper topography had more groundwater contributing to streamflow, but this groundwater was younger. We predict that under future climate scenarios, streams in areas with steep topography and young groundwater are more likely to dry.

1. Introduction

Headwater streams support riparian ecosystems and control downstream water quantity, nutrients, and solutes (Wohl, 2017), but are subject to changes in water quantity and quality as climate change impacts groundwater recharge patterns. In the western U.S., winter snow is the main source of recharge in many mountain catchments. Infiltrating snowmelt is predicted to shift in both timing and magnitude in the latter half of the 21st century as warmer temperatures cause earlier spring snowmelt and increase the elevation of the rain-snow transition zone (Meixner et al., 2016), thus shifting the primary form of winter precipitation from snow to rain in many areas (Klos et al., 2014). In addition, snow water equivalent declines of ~25% in the western U.S. are expected by 2050 (Siirila-Woodburn et al., 2021). These recharge changes are expected to impact groundwater availability (Cuthbert et al., 2019), and subsequently the timing and magnitude of transpiration (Christensen et al., 2008; Stephens et al., 2022). Currently, the impacts of changing recharge patterns on groundwater levels and streamflow are ambiguous because of uncertainty in both controls on groundwater-surface water connection

and future climate projections (Blöschl et al., 2019; Meixner et al., 2016; Musselman et al., 2021; Segura, 2021; Siirila-Woodburn et al., 2021; Zapata-Rios et al., 2016). As a result, hydrologists are still working to predict how headwater streamflow quantity and quality will respond to a changing climate.

Annual stream discharge and precipitation magnitude are closely linked, but during seasonal dry periods and drought groundwater often sustains streamflow in arid and semi-arid regions (Hale & McDonnell, 2016; Hood et al., 2006; Winter et al., 1998; Zaremehrjardy et al., 2022). Changes in the timing and source of infiltrating water with a changing climate are expected to decrease groundwater recharge because transient rainfall infiltrates less effectively than slow-melting snow (Earman & Dettinger, 2011; Siirila-Woodburn et al., 2021). As a result, there is potential for groundwater levels to decline under a changing climate (Siirila-Woodburn et al., 2021) and subsequently decrease groundwater's contribution to streams.

Characterizing watershed groundwater systems is critical to predicting future groundwater resources as there is a relation between the residence time of water in a catchment and the timescale of a catchment's response to perturbations (Althaus et al., 2009; Green et al., 2021; Jurgens et al., 2022; Katsuyama et al., 2010; Meyers et al., 2021; Rademacher et al., 2005). Quantifying groundwater contribution to streams is important for predicting future streamflow and water quality, and thus future impacts to water resources and stream ecosystems. Groundwater residence-time studies can inform predictions of groundwater response to climate change by elucidating when and where water is recharged, how groundwater is stored, and how groundwater moves through a catchment (Urióstegui et al., 2017). Even in mountainous watersheds with frequent turnover, groundwater can be years to decades old and is an important control on runoff generation (Abbott et al., 2016; Manning et al., 2021; Sprenger et al., 2018). Quantifying this watershed response is important, as steady groundwater storage and discharge are critical to maintaining catchment water balances and streamflow.

Groundwater's role in stream systems is further complicated by the fact that up to 50% of streams in the global river network periodically cease to flow as intermittent streams (Datry et al., 2014), and this number is expected to increase in future climate scenarios (Moidu et al., 2021; Reynolds et al., 2015; Sauquet et al., 2021). Predicting future stream permanence is important as persistent streamflow is vital to water quality and quantity (Shanafield et al., 2021), as well as stream and riparian ecological (Acuña et al., 2017; Stubbington et al., 2017) and biogeochemical processes (Datry et al., 2014; Fovet et al., 2021). Even in a small headwater catchment, groundwater support to surface flow can vary significantly through both time and space, leading to drying (Dohman et al., 2021; Warix et al., 2021). For headwater streams to persist under future drought conditions, ample, well-connected groundwater will likely be required. However, hydrologists cannot currently predict how stream intermittency will change in the future because physical watershed properties that favor well-connected groundwater are heterogeneous and difficult and labor intensive to measure directly.

Groundwater contribution to streams is dependent on watershed topography, hydraulic gradients, and hydraulic conductivity (Gleeson & Manning, 2008; Marçais et al., 2022; Sprenger et al., 2019; White et al., 2021; Winter 2001), all factors which vary with space, scale, and time. Watershed topography has been observed to impact where water accumulates within valley networks and is hypothesized to modulate flow partitioning between the surface and subsurface as determined by stream expansion and contraction. McGuire et al. (2005) established a connection between stream residence time and topography at the multi-catchment scale, which we build upon here by incorporating groundwater residence time and streambed hydraulic conductivity, within a single catchment, to make predictions about response to future climate. Streambed hydraulic conductivity influences the connection between groundwater and streamflow (Brunner et al., 2009; Quichimbo et al., 2020; Tripathi et al., 2021), but it is difficult to measure at fine spatial scales due to heterogeneity at multiple scales and difficulty in obtaining direct observations. To accurately predict how groundwater support to streams will change in the future, we look to identify physical watershed properties that are predictive of a stable groundwater-surface water connection.

In this paper, we identified correlations between topography, streambed hydraulic conductivity, groundwater residence times, and groundwater-surface water connection at eight different locations in a single mountainous headwater catchment in the western U.S. to identify groundwater support of streamflow. We ask: (a) what physical properties are correlated with spatial and temporal variations in the age of groundwater contributing to surface flows? and (b) how does groundwater-surface connection control near-stream groundwater age and potential for future stream drying? Our goals are to provide a foundation for identifying watershed properties predictive of stream drying patterns at local scales, and how stream intermittency patterns may shift under a changing climate.

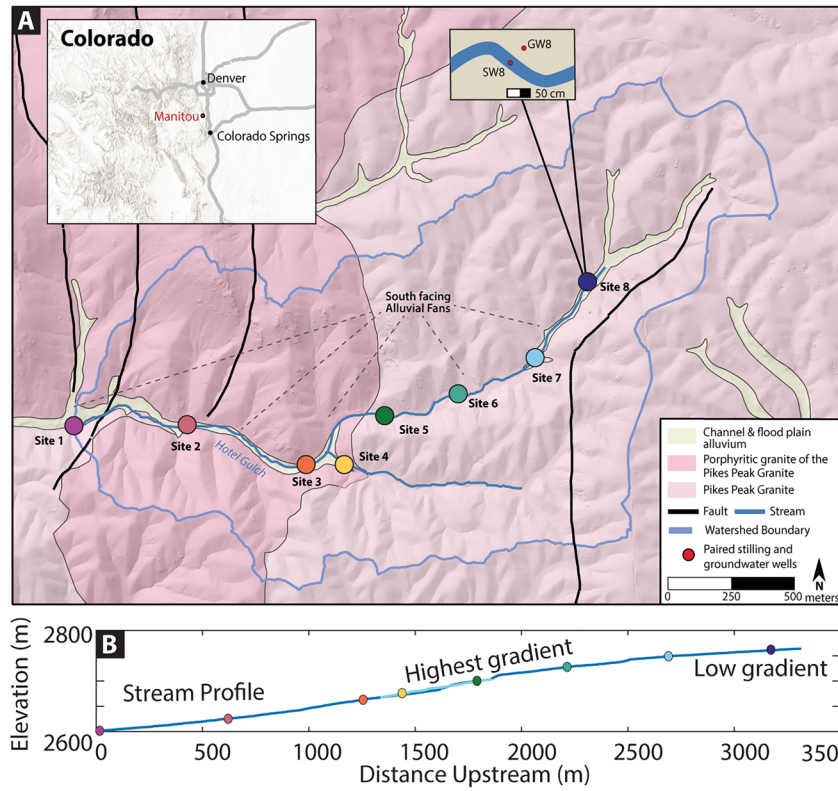

Figure 1. (a) Map of sampling locations within the Hotel Gulch watershed, Manitou Experimental Forest, Colorado, USA. Paired stilling wells and groundwater wells (GW) are displayed as multicolored dots, with a stream inset at Site 8 showing the relative locations of the stilling wells and GW as red dots. All GW are located within a meter of the north bank of the stream. (b) Stream profile showing that the upper watershed has lower hydraulic gradient as compared to the central watershed where stream gradient is relatively steeper.

2. Site Description

This study was completed in the upper Hotel Gulch watershed within the Manitou Experimental Forest CO, United States (Figure 1). This area is part of the greater Front Range province and approximately 20 miles northwest of Colorado Springs, CO. We instrumented eight sites within the watershed with a paired stilling well and a near-stream, shallow, groundwater piezometer. Sites are numbered from the lowest elevation to the highest (Site 1 through Site 8) and at each site stilling wells are referred to as SW(n) and groundwater piezometers are referred to as GW(n) where n is the site number (Table 1). Seven of these sites are located along the main stem with Site 4 located on a small tributary that discharges to the main stem upstream of Site 3 (Figure 1).

The catchment is 3 km^2 and the main stem of Hotel Gulch is 2 km long with a stream width range of 20–60 cm. Hotel Gulch is a small, first-order headwater stream, and from April to November 2021, the average outlet discharge was 4 L/s. The climate is semi-arid with a mean annual precipitation of 36 cm (1979–2021) (NADP, 2022). The Hotel Gulch watershed has steep, densely vegetated, north-facing slopes, and more gradual, relatively sparsely vegetated south-facing slopes. Vegetation consists of pine, mixed conifers, and aspen groves, as well as near-stream riparian vegetation such as willows. The south-facing slopes have several alluvial fan features that cut through south-facing hillslopes and extend to the stream corridor (Figure 1). Site 1, in the lowest portion of the watershed, has an average slope within an upstream 100-m radius <19°. The middle of the watershed (Sites 2–6) is incised with steeper near-stream slopes ranging from 17° to 26°. Upstream of Site 7, the stream corridor extends into a broad floodplain and the near-stream topography is flat, relative to downstream sections (average slope within an upstream 100-m radius <14.5°).

The Hotel Gulch watershed is underlain by two granite members of the Pikes Peak batholith. The upper portion of the watershed is underlain by porphyritic granite of the Pikes Peak batholith (Ypb), while the lower portion is underlain by the Pikes Peak granite (Ypp) (Temple et al., 2007; Figure 1). The two granite members are similar in

Table 1
Table With Groundwater (GW) and Surface Water (SW) Well Coordinates, Elevation, Upstream Area, Slope, Discharge (Q) Measured in June and September, and the Average Modeled Hydraulic Conductivity (K)

Site ID	GW longitude	GW latitude	SW longitude	SW latitude	SW elevation (m)	Upstream area (km^2)	Slope 100-m upstream buffer (°)	Q 6/10/21 (L/s)	Q 9/25/21 (L/s)	Modeled K (m/s)
1	−105.054215	39.0894044	−105.0542	39.0894045	2,601	3.1	18.9	4.8	1.2	2E−06
2	−105.048857	39.0894717	−105.04887	39.0894498	2,625	2.7	23.6	3.0	0.0	1E−03
3	−105.043235	39.0880495	−105.04323	39.0880599	2,663	2.3	22.0	1.9	1.1	2E−06
4	−105.041482	39.0880009	−105.04146	39.0880027	2,676	0.6	22.8	0.4	0.5	1E−05
5	−105.039514	39.0899068	−105.03948	39.0898721	2,700	1.3	26.2	0.4	0.1	2E−04
6	−105.035907	39.0906293	−105.0359	39.0906297	2,728	1.0	17.4	1.8	0.4	3E−05
7	−105.032372	39.0919627	−105.03232	39.0919573	2,749	0.9	14.2	0.9	0.2	3E−06
8	−105.029803	39.0946216	−105.02979	39.0946217	2,761	0.6	13.5	0.7	0.5	2E−07

Note. Slope was calculated by creating a 100-m semi-circle buffer upstream of each well and calculating the average slope within the polygon. The semi-circle was cut so that the diameter is perpendicular to the stream.

composition—a hornblende-bearing biotite granite—and primarily vary in crystal size. The constituent minerals include microcline (35%–50%), quartz (20%–35%), plagioclase (10%–20%), biotite (2%–7%), and hornblende (0.5%–2%) (Temple et al., 2007). Accessory minerals include zircon, apatite, magnetite, and fluorite (Temple et al., 2007; Wanty et al., 1992). The Pikes Peak granite is a fractured system (Blair, 1976), and fractures control groundwater flow (Wanty et al., 1992). Four north-south trending faults cut or approach the stream as part of the Mount Deception Fault System (Temple et al., 2007; Figure 1).

A series of three faults is mapped near the watershed outlet and Sites 1 and 2. The fault closest to Site 1 is projected across the stream bed, the other two are mapped with a terminus prior to crossing the stream bed. The comparatively small changes in discharge after storm events at Site 1, relative to other sites, as well as relatively low stream temperatures from a longitudinal survey of stream temperature (Figure S1 in Supporting Information S1) suggest that faulting influences streamflow at Site 1. At and around Site 2, the stream was observed to dry in August, September, and October 2021. Sites 7 and 8 are the farthest upstream and are located in a relatively flat portion of the watershed (Figure 1). Another fault is mapped at the upper reaches of the watershed along the south slope. Groundwater seeps are common in this upper portion of the watershed and the floodplain is wider than in the lower portions of the catchment.

Soils in the watershed include aquolls in the riparian zone and very gravelly coarse sandy loam to gravelly coarse sandy loam on hillslopes (R. Moore, 1992; Soil Survey Staff et al., 2023). Detailed information about variability in regolith thickness does not exist for the Manitou Experimental Forest; however, the maximum soil profile thickness for mapped soil units in the watershed is 1.55 m (R. Moore, 1992). While installing riparian piezometers we achieved depth to refusal at approximately 1.5–2 me deep for Sites 1–6 but did not reach refusal at Sites 7 and 8, indicating thicker regolith in the riparian zone of the upper watershed. In this upper portion of the watershed, we observed that soil in the riparian zone has a greater fraction of silt and clay relative to the lower portion of the catchment, which is mostly composed of sand and gravel. This higher fraction of silt and clay leads to lower hydraulic conductivity in the upper catchment, and this part of the field system contains numerous diffuse groundwater seeps and pooled surface water. Channel and floodplain alluvium have been mapped throughout the riparian zone. These sediments consist of angular to sub-rounded pebble gravel and sand and are estimated to be 0.6–1.7 m thick (Temple et al., 2007). We also observed fluorite grains in riparian soils (Figure S2 in Supporting Information S1).

3. Methods

To characterize spatial and temporal heterogeneity in the connection between groundwater and surface water we measured: (a) surface water discharge and specific conductivity time series; (b) groundwater level and specific conductivity time series; (c) stream fluoride concentrations, used in an end-member mixing analysis to estimate groundwater fractions to streamflow as described below; (d) groundwater chlorofluorocarbons (CFCs) and

tritium (^{3}H) for residence time estimations; (e) streambed hydraulic conductivity; and (f) watershed topography. Figure S3 in Supporting Information S1 is a summary of the methods used for groundwater age calculations and surface water end-member mixing.

3.1. Time-Series Data Collection

3.1.1. Stilling Wells, Discharge, and Precipitation

We instrumented eight stilling wells throughout the stream with 5.1-cm (2-inch) PVC. Stream electrical conductivity was recorded by HOBO U24-001 loggers every 15 min from 10 April to 6 November 2021, and was converted to specific conductivity. We hung HOBO U20 level loggers in each stilling well to record total pressure every 15 min over the same time period. Total pressure was converted to water level using air pressure recorded with HOBO U20 level loggers hung in trees near Site 1 and Site 8.

We paired manual discharge measurements with stilling well observations to create rating curves at each of the eight sites. Manual discharge was measured 12 times at all sites except Site 4, where it was measured 14 times. Discharge was measured using the salt dilution method as described in R. D. D. Moore (2005) with NaCl. A large rainstorm in early August changed channel morphology and necessitated development of a secondary rating curve at Site 4 for after the storm. Two rating curves also are used at Site 2, where early season ice (10 April–15 May) altered channel morphology. Because we do not have physical discharge measurements at high flows after storm events, we did not calculate discharge if the measured stage was more than 1 cm higher than the maximum stage recorded. 2.2% of stage observations were set to null values instead of being converted to discharge because of lack of high-discharge measurements.

Weekly precipitation was downloaded from then NADP from Site CO21 (NADP, 2022), located ∼2 miles west of our most downstream location (Site 1).

3.1.2. Groundwater Wells

Shallow, hand-installed, streambank wells provide an effective, low-cost means of directly characterizing the chemistry and age of groundwater discharge to gaining mountain streams, and have been increasingly used in recent studies for this purpose (e.g., Manning et al., 2022). We installed eight shallow piezometers with 3.8-cm (1.5-inch) PVC within a meter of the stream bank, adjacent to each of the eight stilling wells. Wells were installed with an auger and drive-point rod. Groundwater wells (GW) at Sites 1–6 were installed into sandy gravel with interspersed cobbles. In contrast, wells at Sites 7 and 8 were installed into clay and silt interspersed with sand and gravel. Well depths ranged from 1.0 to 1.8 m, depending on the depth to refusal, and water levels in the wells were generally <0.5 m. The refusal depths and maximum mapped soil thicknesses of <2 m (R. Moore, 1992) suggest that the wells likely transect a significant fraction of the saturated regolith thickness. The bottom 80% of each well was screened to capture all flowlines reaching the well with screens that spanned nearly the full saturated thickness of the regolith. The water table was below the top of the screen for 67% of groundwater age samples before pumping started. For all well samples, the water table dropped during pumping, typically below the top of the screen, suggesting that we captured the majority of flow lines reaching the stream. We assume that the wells intercept most of groundwater discharging to the stream from the right bank at the well location, given that well depths generally exceed stream widths by a factor of 2–3. Well water had solute concentrations greater than adjacent surface water, and we did not observe specific conductivity spikes in the wells after salt dilution tracer tests. These two observations suggest that the wells contain minimal surface water lost from the stream. Each well contained a HOBO U24-001 electrical conductivity logger and a HOBO U20 water level logger that recorded every 15 min from 10 June to 6 November 2021.

3.1.3. Stream and Groundwater Chemistry

Surface water and groundwater chemistry samples were collected approximately twice a month from June to November 2021 with additional surface water samples collected from April to June 2021. Chemistry samples were collected before salt dilution discharge gauging was completed and GW were purged until well temperature, pH, and specific conductivity were constant. Samples were collected with Viton tubing and a peristaltic pump in 30-mL HDPE Nalgene bottles and were filtered to 0.2 μm with nylon syringes. The pump intake was located approximately 5-cm above the bottom of each well during sampling. One blank and duplicate were collected each sampling day. We measured F^- by ion chromatography and samples were frozen until analysis. Stream and

groundwater pH, specific conductivity, and temperature were determined in the field with a Thermo Fisher Orion Star A329 portable multiparameter meter.

3.2. Groundwater Input Endmember Mixing

Groundwater inputs to stream discharge have been classically estimated using a mass-balance approach informed by two endmembers representing groundwater and runoff (Pinder & Jones, 1969; Sklash et al., 1976). Rather than using water isotopes (Sklash et al., 1976) or specific conductivity (Miller et al., 2014; Saraiva Okello et al., 2018) to define endmembers, as common in other mass-balance-based hydrograph separation, we build upon this approach by using the chemical saturation of precipitation, groundwater, and surface water with respect to fluorite to inform endmembers. Chemical saturation of a bedrock mineral is often not a choice because there are few bedrock minerals with simple chemical formulae that contain elements that are not also in precipitation. However, in this system the presence of fluorite provided a unique opportunity to use the chemical saturation of the groundwater with respect to fluorite as an endmember representation of groundwater. We assumed that streamflow is a mix of two water sources, with endmembers representing recently infiltrated precipitation, and groundwater. Fluorite was chosen because the Pikes Peak granite has anomalously high fluorite (CaF_2) concentrations at 0.35 wt. % (Wanty et al., 1992). When weathered, fluorite dissociates to fluoride and calcium:

$$CaF_2 \rightarrow Ca^{2+} + 2F^{-}$$

delivering fluoride as solute that in an undisturbed system such as Manitou, can only be plausibly sourced from water-rock interactions in the subsurface as fluoride is not commonly found in atmospheric deposition or other pedogenic or geogenic sources.

We used fluoride concentrations to calculate the amount of stream discharge from groundwater (Q_{GW}, L/s) when chemistry samples were collected, following methods from Miller et al. (2014):

$$Q_{GW} = Q_{SW} * \left(\frac{F_{SW} - F_P}{F_{GW} - F_P} \right)$$

where, Q_{SW} (L/s) is the measured stream discharge, F_{SW} (mol/L) is the measured fluoride concentration in streamflow, F_P (mol/L) is the concentration of fluoride in the precipitation endmember, and F_{GW} (mol/L) is the concentration of fluoride at saturation with fluorite for the groundwater endmember. We computed the mean area-weighted groundwater discharge for each site by taking the average of all Q_{GW} values for each site and dividing by the upstream area.

The precipitation component to flow represents rain and snow that have entered the shallow subsurface and are not geochemically evolved, representing water that has been in the subsurface for less than a year. We assumed very dilute fluoride in precipitation with $[F^-] = 1 \times 10^{-10}$ mol/L. A nearby NADP site (Site CO21) exists at the Manitou Experimental Forest headquarters, but it does not report fluoride chemistry.

The groundwater endmember represents all groundwater contributing to streamflow. This includes any water that has spent enough time in the subsurface to weather fluorite and accumulate dissolved fluoride. It does not distinguish between bedrock and regolith storage, but instead encapsulates groundwater flow that has reached saturation with fluorite and may include a range of groundwater sources such as deep fracture flow, groundwater stored in regolith, and interflow, as long as fluorite saturation has been reached.

To determine the groundwater endmember, we first calculated the chemical saturation of groundwater samples with respect to fluorite for samples that had a stoichiometry ratio of 2F:Ca, based on the mineral formula for Fluorite (CaF_2). We observed that groundwater was chemically saturated with respect to fluorite at some point during the season at every site location. We reported the potential range and mean of groundwater discharge and fraction of total streamflow, based on the range of fluoride concentrations at saturation with fluorite. To further validate this endmember assumption, we then created a 1D reactive transport model with CrunchTope to evaluate the residence times required for water to reach saturation with respect to fluorite. We observed that 1D flow reached fluorite saturation at 1.5 years residence time (Figure S4 in Supporting Information S1), well within the observed groundwater residence times at Manitou, and thus it is reasonable to expect that groundwater contributing to surface water in Hotel Gulch is saturated with respect to fluorite. Any water that is not fully saturated with

respect to fluorite represents a mix of dilute precipitation with an evolved groundwater source. Furthermore, at all eight sites we observed chemostatic concentration-discharge patterns for fluoride, leading to the assumption that fluorite dissolution and fluoride concentrations in streams are at steady state. If streamflow was supersaturated with fluorite, leading to a fraction of discharge from groundwater >100%, we assumed that all stream discharge was sourced from groundwater. Fluorite supersaturation only occurred once for the upper limit of one date at Site 7. There is not a relation between fluoride concentrations in soils and plants (Weinstein, 1977), suggesting that plants do not typically uptake fluoride. We do not see geochemical evidence of evaporation, so conclude that ET is unlikely to be an important process in determining stream fluoride concentrations.

Our endmember mixing analysis does not contain a soil endmember. However, Bush et al. (2023) measured riparian soil fluoride concentrations at several locations throughout the Hotel Gulch catchment. They observed that shallow soil water (10-cm below the surface) was undersaturated with fluorite and had an average saturation index of −0.96 and that fluorite saturation increased with depth in soils. Our average surface water and groundwater fluorite saturation indices were −0.18 and −0.04, respectively. These data show that fluorite saturation in soil water is distinct from surface water and groundwater, and more closely resembles precipitation. Within our endmember mixing model, this dilute soil water would be attributed to the precipitation endmember as it is geochemically unevolved from a fluorite saturation perspective and is likely sourced from recently infiltrated precipitation or snowmelt. We observed visible fluorite grains in regolith samples, indicating that fluorite is present in the regolith.

While we assign no age to the precipitation and groundwater endmembers, they represent relatively young and old components to streamflow, but are independent of the young and old fraction to flow used in the groundwater age calculation in Section 3.5 as they are informed by different data. Our reactive transport model shows that fluorite saturation is reached within 1.5 years (Figure S4 in Supporting Information S1), so groundwater represents water that recharged before the 2021 snowmelt period. Endmembers are based on observed behavior captured over a 1-year period and assumes that other water years have comparable precipitation and groundwater chemistry. We also note that none of the collected hand-samples occurred during an active storm, and thus we do not capture or attempt to estimate unique flowpaths that may be present during storm events.

Another potential limitation of this EMMA analysis is that it does not account for areas of the stream that may be losing, and assumes that groundwater is always contributing to streamflow. If the stream is losing at our sampling locations, we assume that the losing water is well-mixed from a geochemical perspective, and thus matches the chemistry of water we captured in the stream. As a result, EMMA mixing results provide a reliable estimate for the fraction of streamflow from groundwater because it only relies on stream fluoride concentrations and is normalized to the amount of total stream discharge which would be the only variable metric that is influenced by a losing stream, under the assumption above. Regardless, we did not attempt to filter results to only gaining reaches because our Sites are 500 m apart and may have many gaining and losing sections between our sample locations; others have observed gaining/losing stream sections to vary over their lengths (Kasahara & Wondzell, 2003; Rosenberry et al., 2021).

3.3. Hydraulic Conductivity

Streambed hydraulic conductivity was estimated using 1DTempPro (Voytek et al., 2014) informed by temperature measurements collected with thermochron iButtons (DS1925L-F5, measurement error = 0.0625°C). Three iButtons were secured to wood stakes and temperature was recorded every 15-min at the stream bed, 10-cm below the stream, and 20-cm below the stream at each of the eight locations from 0:00 28 May 2022 to 0:00 7 June 2022 (Figure S5 in Supporting Information S1). At Site 7 the 20-cm iButton was water damaged so we used temperature at 1.43-m measured with a U20 Onset HOBO recording at the same time interval in the screened PVC.

1DTempPro numerically solves the flow and heat-transport equations and has a GUI that enables users to calibrate with Variably Saturated 2-Dimensional Heat Transport code to estimate hydraulic conductivity where head is known. The user must provide initial estimates for a change in head between boundary conditions, hydraulic conductivity, porosity, thermal conductivity, heat capacity, and dispersivity. We used the same values for porosity (0.4), thermal conductivity (1 W/m°C), and heat capacity (3.7E+06 W/m°C) at all eight sites, based on pre-programmed data in 1DTempPro data library. We started with a change in head of 1 cm and varied the starting hydraulic conductivity and dispersivity for each sample in an iterative solving approach to find starting

values that enabled the model to converge. All model inputs and outputs, example iButton temperature data, and a conceptual diagram illustrating experiment set-up are present in Supporting Information S1.

3.4. Watershed Topography

We used 1-m LiDAR for all topographic analysis and watershed delineation (Rossi et al., 2022). The watershed boundary and upstream accumulated area was determined using watershed function tools in ArcGIS Pro. We used the slope tool in ArcGIS Pro to calculate slope from LiDAR. We then created a circular buffer around each well to calculate slope for a variety of contributing areas. Because unconfined groundwater often loosely mirrors topography, we split each buffer into a semi-circle cut perpendicular to the direction of flow at the stream adjacent to each well to avoid downgradient topography impacting the slope of contributing area (Figure S6 in Supporting Information S1). We then averaged the slope within the semi-circle polygon using the zonal statistics tool. Average slope was calculated in 5, 10, 20, 30, 50, and 100-m intervals and relative changes in slope between sites scaled similarly across the eight sites regardless of buffer length, as indicated by simple linear regression. We used a 100-m radius for statistical analysis because it captured the change in slope between the valley and adjacent hillslopes adjacent to the stream at all sites, whereas some of the smaller intervals were not wide enough to capture the break and slope at Sites 7 and 8, based on visual inspection.

3.5. Groundwater Age Sampling and Calculations

Samples were collected for chlorofluorocarbons (CFC-11, CFC-12, and CFC-113) and tritium (^{3}H) to constrain groundwater age, and for dissolved concentrations of N_2 and Ar gases to compute the recharge temperature and excess air parameters required for age calculations. The first round of age-tracer sampling took place on 9–10 June 2021, including N_2/Ar gases, CFCs, and tritium samples (Table S2 in Supporting Information S1). On 24–25 September a second round of CFC and tritium samples were collected, except for at Site 2 where low groundwater levels prevented collection of a reliable sample (Table S2 in Supporting Information S1). All samples were collected using a peristaltic pump and Viton tubing. The pump intake was placed near the bottom of the water column (approximately 5-cm above the bottom of the well) to maintain hydraulic pressure on sampled water and minimize the potential for dissolved gas loss from bubble formation during pumping.

Nitrogen and argon gas samples were collected in duplicate 250-mL glass bottles with rubber stoppers following methods described by the U.S. Geological Survey (USGS) Reston Groundwater Dating laboratory (USGS, 2021), where they were analyzed. CFC samples were collected in triplicate in 500-mL glass bottles sealed with foil caps and tritium samples were collected in 1-L HDPE Nalgene bottles, both consistent with methods described by the University of Miami Tritium Laboratory (University of Miami Tritium Laboratory, 2021), where they were analyzed.

Equilibrium atmospheric mixing ratios in parts per trillion by volume (pptv) were computed for the measured CFC concentrations (Table S2 in Supporting Information S1) using standard methods described in Busenberg and Plummer (1992) and Plummer and Busenberg (2000). The recharge elevation was assumed to be the mean elevation of the total contributing area to each well as described above. Recharge temperature and excess air were computed from N_2 and Ar concentrations (Table S2 in Supporting Information S1) using the method described in Busenberg et al. (1993), which assumes the unfractionated air model of excess air formation (Aeschbach-Hertig et al., 2000). Excess N_2 from denitrification was not suspected and assumed to be negligible. Computed recharge temperatures range from 2.4° to 6.2°C, with a mean of 4.6°C, consistent with the site's mean annual air temperature of 5°C (Manning, 2011; Seltzer et al., 2021). Computed excess air concentrations are 0.1–1.8 cm^{3}STP/L, within the normal range for groundwater (Stute & Schlosser, 2000). Recharge temperatures and excess air concentrations for the September CFC samples were assumed equal to those computed from N_2 and Ar gas concentrations in the June samples because N_2/Ar samples were not collected in September.

We used both CFC-12 and tritium to estimate a mean groundwater age for each sample, employing the TracerLPM calculator (Jurgens et al., 2012). CFC-11 and CFC-113 were not used given their greater potential for degradation under low-oxygen conditions (Bockgård et al., 2004; Sebol et al., 2007); all wells had dissolved oxygen concentrations ≤1 mg/L, as determined with CHEMets kits (K-7512) during sampling. June CFC-12 data at Site 7 and September CFC-12 data at Sites 3 and 7 were not reported due to large SF_6 chromatogram peaks that obscured the CFC-12 peak. For these samples, we estimated the CFC-12 equilibrium atmospheric mixing

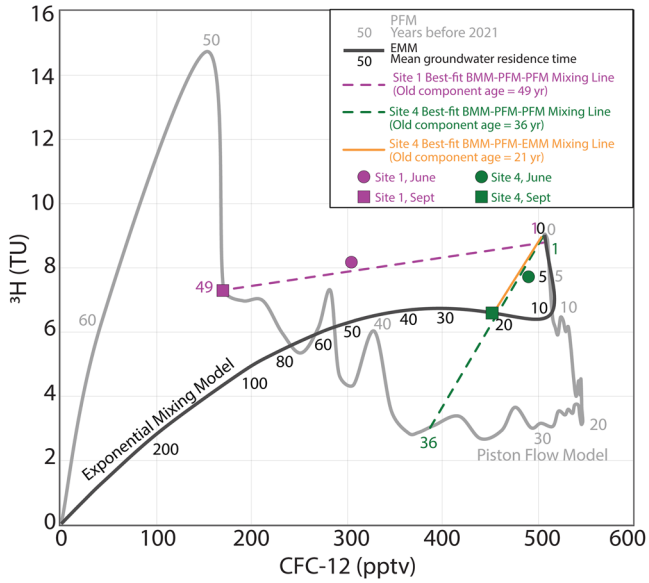

Figure 2. Plot of ^{3}H concentration (decayed to the sample year, 2021) versus CFC-12 equilibrium atmospheric mixing ratio illustrating the approach used to compute older fraction age, young water fraction, and sample mean age for samples in this study. Lines are shown corresponding to the piston flow model and exponential mixing model. Sample points and corresponding best-fit bimodal mixing model lines are shown for Sites 1 and 4.

ratio based on the CFC-113 value, given the consistent relation between CFC-113 and CFC-12 mixing ratios observed for all other samples. Regression lines for plots of CFC-12 versus CFC-113 mixing ratio had an $R^2 = 0.96$ and p-value = 0.0001 for June samples and $R^2 = 0.88$ and p-value = 0.007 for September samples (Figure S7 in Supporting Information S1). Historical atmospheric CFC-12 mixing ratios used in TracerLPM were obtained from the USGS Groundwater Dating Lab website (USGS, 2021). The precipitation tritium concentration record used was derived from the regional estimates in Jurgens (2018). Estimates provided for the site location for the years 1953–2012 were extended forward to 2021 by correlation with the precipitation tritium record for Vienna, Austria (International Atomic Energy Agency's Global Network of Isotopes in Precipitation, https://www.iaea.org/services/networks/gnip) using correlation coefficients provided in Jurgens (2018) for this purpose.

Sample mean ages were initially evaluated assuming the two simplest and commonly applied age distribution models, the piston flow model (PFM) and exponential mixing model (EMM, Cook & Böhlke, 2000). The PFM assumes that all water in the sample is of uniform age. The EMM assumes sampled water is discharging from the toe of a simple hillslope aquifer having uniform thickness, porosity, and recharge, and has been widely assumed in catchment travel time studies (e.g., McGuire & McDonnell, 2006). However, many samples were clearly inconsistent with these two models, plotting off the PFM and EMM model lines on a tracer-tracer plot of tritium concentration versus CFC-12 mixing ratio (Figure 2). A binary mixing model (BMM) including a very young (1 year old) component and an older modern (<70 years old) component of variable age was therefore adopted for the following two reasons. First, the model is conceptually consistent with a watershed underlain by a relatively low-hydraulic-conductivity fractured-bedrock aquifer (providing the older component) with a relatively high-hydraulic-conductivity shallow layer of unconsolidated material on top of it (providing the young component as interflow; Carroll et al., 2019, 2020; Gardner et al., 2020) and has been invoked in prior mountain watershed studies (Manning et al., 2012; Uhlenbrook et al., 2002). Second, for all four wells having substantially different June and September ages (Sites 1, 4, 5, and 6), the line connecting the two samples on the ^{3}H versus CFC-12 plot referred to above projects to the portion of the PFM/EMM lines corresponding to water 0–3 years old, consistent with both samples containing the same older component and different amounts of a young component ~1 year old.

Figure 2 illustrates the approach used to compute the older component age, young fraction magnitude, and sample mean age for each sample, showing Sites 1 and 4 as examples. For each site, a BMM line extending outward from the point on the PFM line corresponding to 1-year-old water was fit to the June and September sample points (dashed lines in Figure 2). The projected intersection of this BMM line with the PFM line was taken as the older component, having ages of 49 and 36 years for Sites 1 and 4, respectively. Because both components are represented by the PFM, this mixing model is referred to here as a BMM-PFM-PFM. The TracerLPM fitting tool was then applied to compute the young water fraction for each of the two samples, this being the relative distance of the sample from the older component along the BMM-PFM-PFM line. For example, young fractions for June and September samples are 0.42 and 0.00 for Site 1, respectively, and 0.75 and 0.57 for Site 4, respectively. In cases where the older component could fall on either PFM or EMM lines, the older component and sample mean ages were also computed for the latter scenario (referred to as a BMM-PFM-EMM). Site 4 presents such a case, and its corresponding BMM-PFM-EMM line is shown as a solid orange line in Figure 2 (older component mean age = 21 years). We acknowledge that in a dynamic headwater system such as Manitou, the age of young and older components may be transient (Popp et al., 2021), and an infinite number of possible mixing scenarios exist for each sample. The BMM's applied above are likely significant simplifications of actual sample age distributions, and more complex and realistic types of age distributions would fit just as well with the sample data. However, on the principle of parsimony, we have selected these BMM's because they are the simplest form of mixing model consistent with both the data set and the hydrologic setting. We also note that, though our data support the samples containing dominantly modern water (otherwise, samples would plot closer to the origin in

Figures 2 and 6a), we cannot rule out the possibility of samples containing some amount of premodern water (>70 years old), given that tracers capable of dating premodern water were not collected.

We report a lab error of ±2 years for CFC PFM ages but did not quantify error associated with sample mean ages (based on ^{3}H and CFC-12) because these were computed based on modeling assumptions and are interpreted estimates. Certainty around the mean ages can be proxied by comparing estimates from different mixing models for a single sample, as provided in Table S3 in Supporting Information S1. We note that while the absolute age of samples varies between flow models, the relative distribution of ages is consistent, and this relative distribution drives our conclusions rather than absolute ages.

3.6. Statistical Analysis

We compared groundwater ages against other variables and used Pearson's rank correlation to compute p-values. Throughout this manuscript, we define statistically significant correlations as those having a p-value less than 0.05. We report Pearson's rho values alongside p-values, calculated using the "corr" function in MATLAB.

4. Results

4.1. Streamflow and Groundwater Observations

4.1.1. Discharge, Groundwater Level, and Specific Conductivity

Stream discharge was consistently highest among the eight sites in early May, during the peak snowmelt period, until late May, when all snow melted (Figure 3). The highest average flows occurred at the farthest downstream location, Site 1. Site 4 is a small tributary stream and had the lowest mean discharge. Site 2 is located near a fault (Figure 1) and was the only location to dry during this period (Figure 3). On 10 June, during the first round of groundwater residence time sampling, the stream was gaining except for between Sites 6 and 5 where stream morphology transitions from broad floodplains and alluvial fans to incised valleys (Table 1; Figure S8 in Supporting Information S1). On 25 September, during groundwater residence time sampling, the stream alternated between gaining and losing with the largest loss at Site 2 where the stream was dry and the largest gain just downstream at Site 1 near a fault (Table 1; Figure S8 in Supporting Information S1).

During June and July, summer monsoon storms caused frequent precipitation events, but the response was not constant throughout the 2-km stream (Figure 3). Site 1 had small responses while Sites 3, 7, and 8 exhibited flashy discharge (Figures 3b, 3d, 3h, and 3i). Precipitation was scarce from August to November and during this time flows were low across all eight sites. Stream specific conductivity was not as dynamic across sites as stream discharge (Figure 3). Stream specific conductivity was lowest across all sites in April and increased throughout the summer. While there were large increases in discharge after precipitation events there were not proportional decreases in stream specific conductivity (Figure 3). In mid-October riparian vegetation began to senesce and stream discharge increased as a result.

Groundwater-table elevation had less variation than stream discharge (Figure 4). Groundwater levels were highest in June and typically decreased during the summer until October, when they started to increase again. We note that groundwater levels and discharge started to increase in the fall as riparian willows started to lose leaves (Figure 4). All sites showed small increases in water level in response to summer rain events, but we note that Site 7 was the least impacted by precipitation (Figure 4g). Site 2 had the largest changes in groundwater level (a decrease of >40 cm), consistent with being the only surface-water site that dried during the summer (Figure 4b). Groundwater specific conductivity increased throughout the summer before decreasing in October at all sites except Site 7 where it was constant throughout the summer (standard deviation = 0.67 μS/cm), despite decreases in water level (Figure 4g). Specific conductivity at Site 1 and Site 6 dropped after every bimonthly pumping event for geochemical sampling, explaining the sharp decreases specific conductivity data at these sites (Figures 4a and 4f). Sites 2 and 3 had specific conductivity behavior inverse to changes in groundwater level (Figures 4b and 4c) exhibiting dilution behavior, while specific conductivity at Site 4 mirrored changes in groundwater level likely due to solute mobilization (Figure 4d).

4.1.2. Groundwater Fraction Endmember Mixing

We used a two-endmember mixing model to quantify streamflow source. 95% of observations from April to November 2021 show that the Hotel Gulch stream had a groundwater contribution greater than 60% (Figure 5).

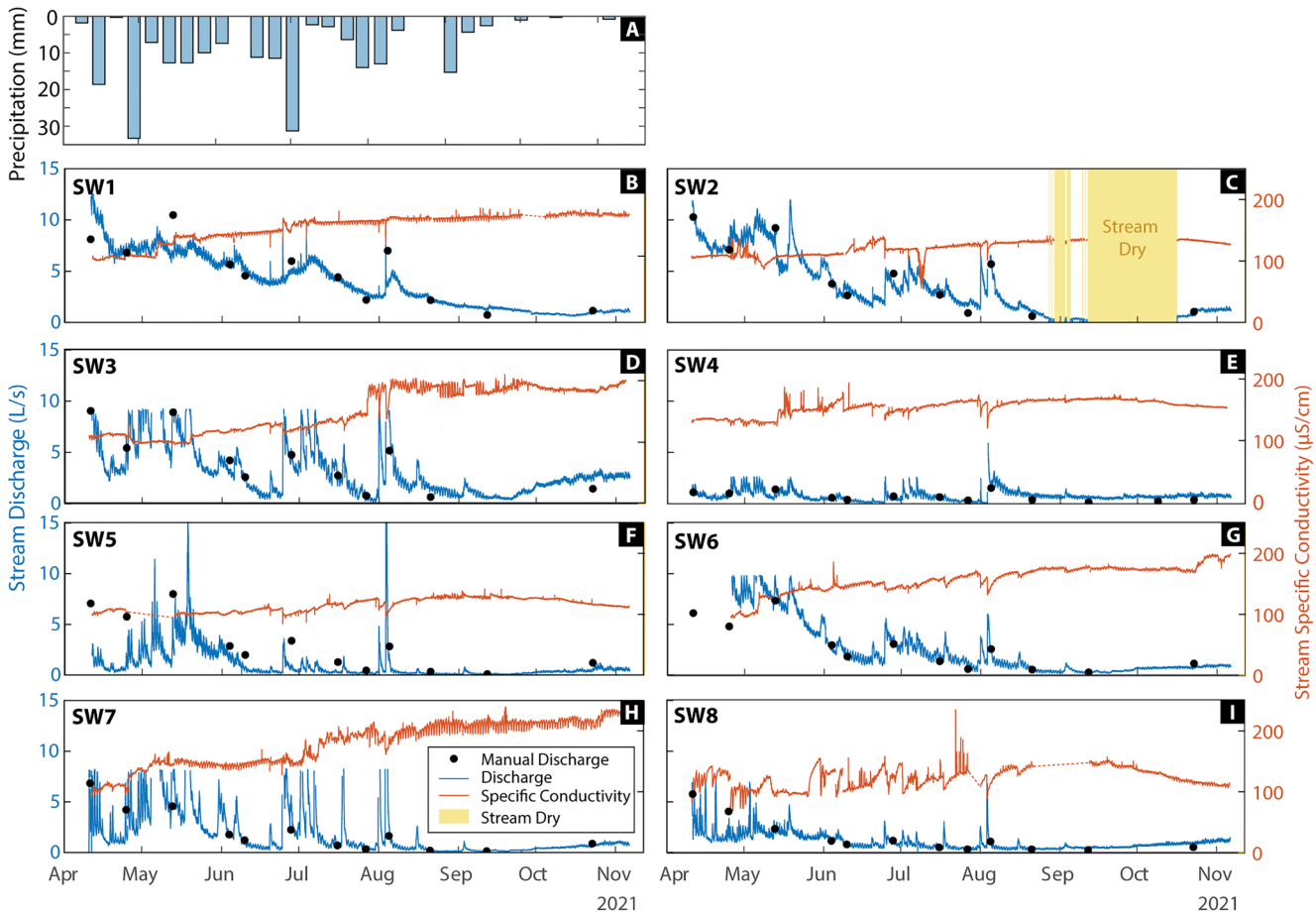

Figure 3. Plots showing stream discharge in blue and specific conductivity in orange from April to November 2021. Precipitation from National Atmospheric Deposition Program site CO21 is displayed in the top left subplot. Linearly interpolated data are shown in a dashed line where data are not available because of datalogger malfunctions, such as for specific conductivity in early October for SW1, late April to early May for SW5, and September for SW8. Manual discharge measurements are displayed as black dots. In early April, some ice was present in the channel at Sites 1 and 5, which caused poor agreement between manual discharge and the rating curve during the first week of the time-series record.

Site 1 has the highest average fraction of discharge from groundwater and is located near two faults (Figure 5a). Sites 5–8 all have a comparatively low (50%–70%) fraction of streamflow from groundwater early in the season while snow was melting, and approach 90% groundwater contribution as the summer progresses (Figures 5e–5h). Sites 7 and 8 have the most dynamic shifts in stream source (Figures 5g and 5h).

4.2. Spatial and Temporal Groundwater Residence Time Trends

The age tracer data are consistent with most of the groundwater samples containing a bimodal mixture of very young (~1 year old) water and older water generally 30–60 years old (Figures 2 and 6a; Table S3 in Supporting Information S1; see Section 3.5). For the four sites with June and September samples of substantially different age (Sites 1, 4, 5, and 6), both the June and September samples plot approximately on a single BMM line including a young component ~1 year old and an older (but still modern) component of some age unique to each set of samples (Figure 6a). We suspect the young component is mainly from interflow within unconsolidated material on top of the bedrock, while the older component is mainly from the bedrock. Table S3 in Supporting Information S1 presents the computed mean age for each sample assuming two different mixing models, including the BMM-PFM-PFM (bimodal with a PFM older component) and, when possible, the BMM-PFM-EMM (bimodal with an EMM older component). The BMM-PFM-PFM is consistent with all samples in the data set. It is therefore considered the preferred model, and all sample mean ages and young endmember fractions discussed below assume this model. Importantly, while the different BMM's produce somewhat different sample mean ages, the

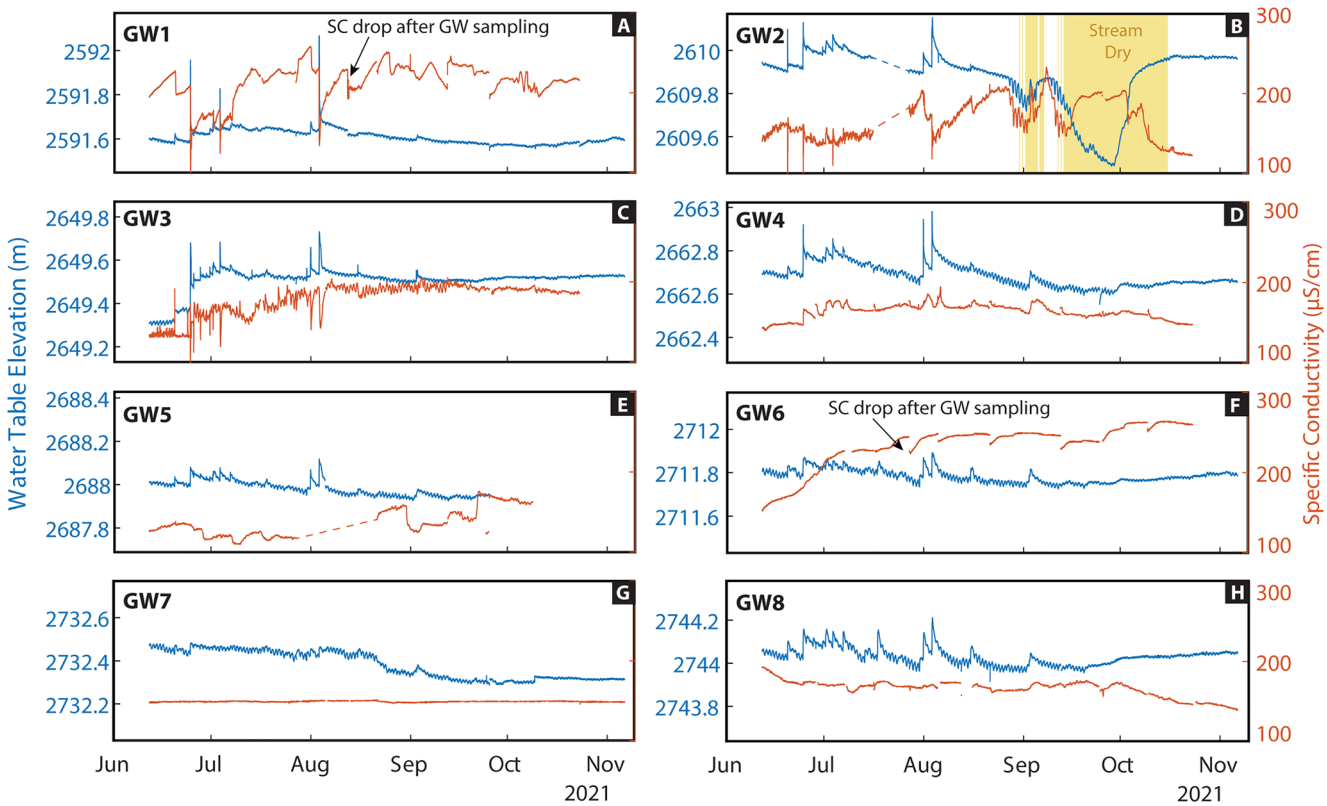

Figure 4. Plots showing groundwater elevation in blue and groundwater specific conductivity in orange from June to November 2021. The left-hand-side *y*-axis limits are different for each subplot due to the change in elevation between sites, but the elevation range (0.8 m) is consistent across plots. The yellow shaded section in panel (b) represents the period when the stream was dry.

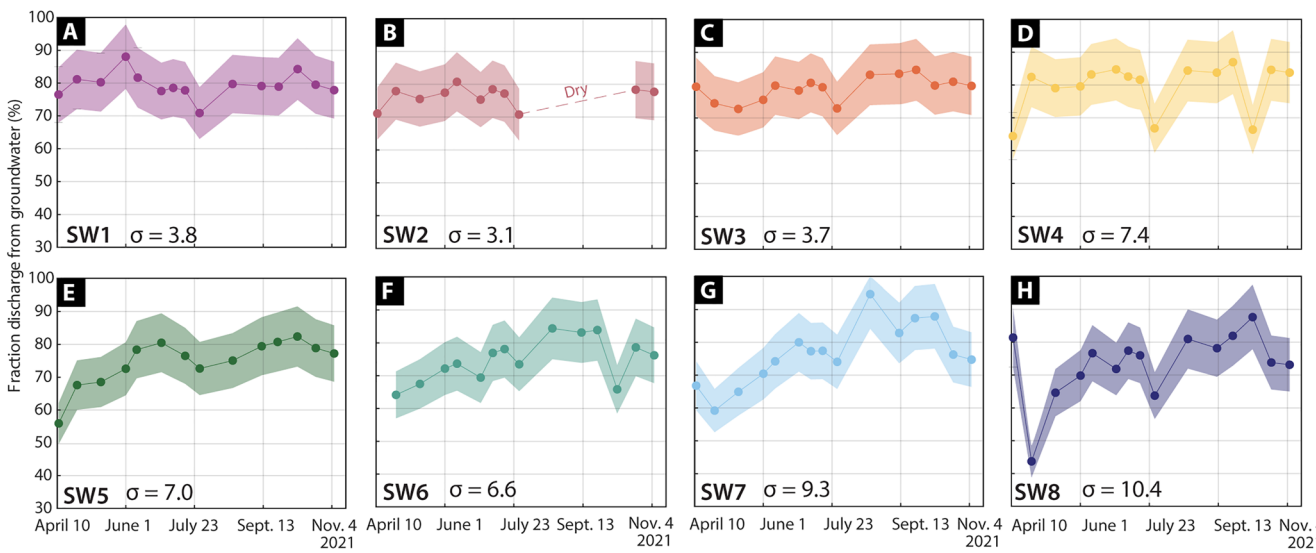

Figure 5. Plots showing the fraction of discharge from groundwater through time at each of the eight surface-water locations. The colored shaded area in each subplot represents the potential range of the fraction of discharge from groundwater, as a function on the minimum and maximum concentrations of fluoride in groundwater endmember (section "Groundwater input endmember mixing"). The plotted points show the midpoint between the potential minimum and maximum values. The standard deviation of all midpoints for each subplot is displayed in the bottom left corner of each subplot. Site 1 had a consistently high and stable fraction of discharge from groundwater, while upper Sites 7 and 8 showed the most variation through time, as indicated by their relatively high standard deviations. Point decreases in the late summer and fall, particularly at upper sites, occurred in the days after large summer monsoon events.

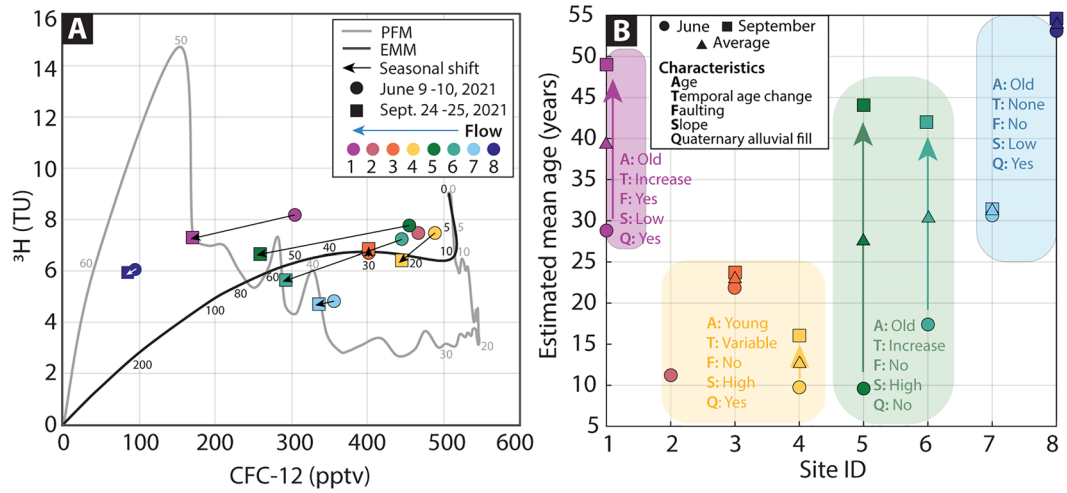

Figure 6. (a) Plot of ^{3}H concentration versus CFC-12 equilibrium atmospheric mixing ratio. Lines corresponding to the piston flow model (PFM) and exponential mixing model (EMM) are shown in addition to all samples. Numbers next to lines show modeled age for PFM and EMM in gray and black, respectively. Samples were collected on 09–10 June 2021 (circles) or 24–25 September 2021 (squares). (b) Estimated best-fit bimodal mixing model-PFM-PFM mean age for samples at each of the eight sites in both June (circles) and September (squares), 2021. The seasonal mean age average (calculated as the average between June and September samples) is also plotted as a triangle. We show colored blocks grouping sites by relative characteristics. These key characteristics are listed by letter for simplicity, including groundwater age (A), the temporal age change from June to September (T), 2021, the presence or absence of faulting through the stream (F), relative changes in local slope (i.e., shallow or steep) (S), and the presence or absence of quaternary alluvial fill (Q).

relative ranking of these mean ages remains approximately the same, and our interpretations below are based mainly on relative age differences between samples rather than absolute ages.

Groundwater-sample mean ages ranged from 10 to 53 years in June and from 16 to 55 years in September (Figure 6b). In June, groundwater residence time was oldest in the upper and lowermost portions of the catchment, while the youngest water was located in the middle of the catchment (Figure 6b, Table S3 in Supporting Information S1). In September, the oldest groundwater was still found in the upper and lower portions of the catchment, but groundwater ages at Sites 5 and 6 were also greater than 40 years. Groundwater ages at Sites 3 and 4 were still relatively young (<25 years) in September (Figure 6b, Table S3 in Supporting Information S1). There was no statistically significant correlation between upstream area and June or September groundwater age (June: $R^2 = 0.04$, p-value = 0.65, September: $R^2 = 0.00$, p-value = 0.96). Site 8 had the oldest water at 53 and 55 years in June and September, respectively. Site 7 is also located in the upper watershed and had older water at 31 years in both June and September. The lowest site, Site 1, is located near a fault and also had relatively old water at 29 and 49 years in June and September, respectively. Groundwater in the middle portion of the catchment (Sites 2–6) had comparatively young ages, ranging from 10 to 24 years, with the exception of September samples from Sites 5 and 6, which were 44 and 42 years, respectively (Suckow et al., 2013).

The largest shifts in residence time between June and September occurred where no alluvial fill is present near the riparian zone, and near the downstream fault (Figure 6b). Sites 1, 4, 5, and 6 had the largest increases in residence time at 20, 13, 34, and 25 years, respectively. The oldest groundwaters, Sites 7 and 8, had the smallest increases in residence time of less than 2 years. The seasonal change in young fraction (Figure 6b) was proportional to the seasonal change in mean age, with the biggest decreases in the young fraction from June to September occurring at Sites 1, 5, and 6. We show no change in groundwater age at Site 2 because groundwater levels were too low to collect a CFC sample in September.

4.3. Relation Between Local Slope, Streambed Hydraulic Conductivity, Groundwater Residence Time, and Groundwater Inputs

Streambed hydraulic conductivity spanned four orders of magnitude, ranging from 1E−03 to 2E−07 m/s throughout the watershed (Figure 7b, Table 1). The highest streambed hydraulic conductivity was found at Site 2

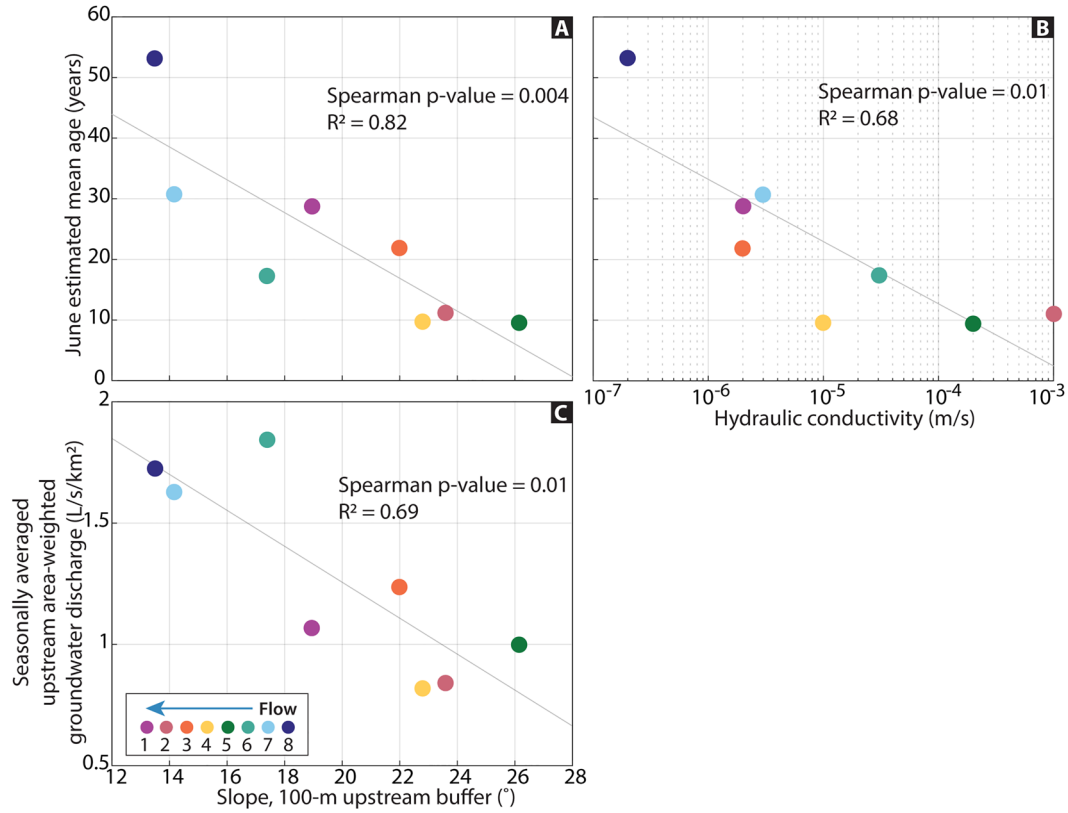

Figure 7. Plots showing the best-fit bimodal mixing model-piston flow model (PFM)-PFM June mean age for each groundwater well plotted against the average slope within a 100-m upstream buffer at each well and (b) the hydraulic conductivity in the shallow streambed at each site. Panel (c) shows a positive correlation between the average slope within a 100-m upstream buffer at each well and the seasonally averaged upstream area-weighted groundwater discharge. All points are colored by their site ID, as consistent with the rest of the manuscript. *P*-values and R^2 values were calculated using Pearson's correlation test. Linear correlation equations are present in the bottom right corner of each plot.

(1E−3 m/s), coinciding with the only location where the stream dried. Sites 8 had the lowest streambed hydraulic conductivity 2E−07 m/s and coincided with where we observed the highest fraction of silt in the streambed. Sites 1–6 ranged from 2E−06 to 2E−04 m/s.

We observed statistically significant correlations between slope in a 100-m upstream buffer, groundwater age, groundwater inputs to streamflow, and streambed hydraulic conductivity (Figure 7). June mean groundwater ages were correlated with the upgradient slope within a 100-m buffer ($R^2 = 0.70$, p-value = 0.009) and the streambed hydraulic conductivity ($R^2 = 0.70$, p-value = 0.009) (Figures 7a and 7b). These relative correlations are also present with September and seasonally weighted mean ages but are not significant at the 0.05 significance level (Figure S9 in Supporting Information S1). We suggest that the June mean ages are more representative of groundwater behavior because most of the stream is gaining in June. In contrast, in September there were several alternating gaining and losing sections throughout the catchment (Figure S8 in Supporting Information S1) that could potentially cause mean ages to appear younger as a result of infiltrating streamflow upgradient. Conclusions throughout the discussion are thus based on June mean ages.

We compared the seasonal mean upstream area-weighted discharge from groundwater (L/s/km^2), as determined by the endmember mixing (section "Groundwater input endmember mixing"), to slope and found that groundwater inputs to streamflow were greater in flat areas (Figure 7c) ($R^2 = 0.69$, p-value = 0.01).

The seasonal change in groundwater age does not correlate with the change in the fraction of discharge from groundwater on the groundwater age sample days. Where there were large changes in the fraction of discharge from groundwater, mean groundwater age was relatively constant (Sites 3, 7, 8, Figure S10 in Supporting Information S1). At sites where groundwater age increased from spring to fall, the fraction of discharge from

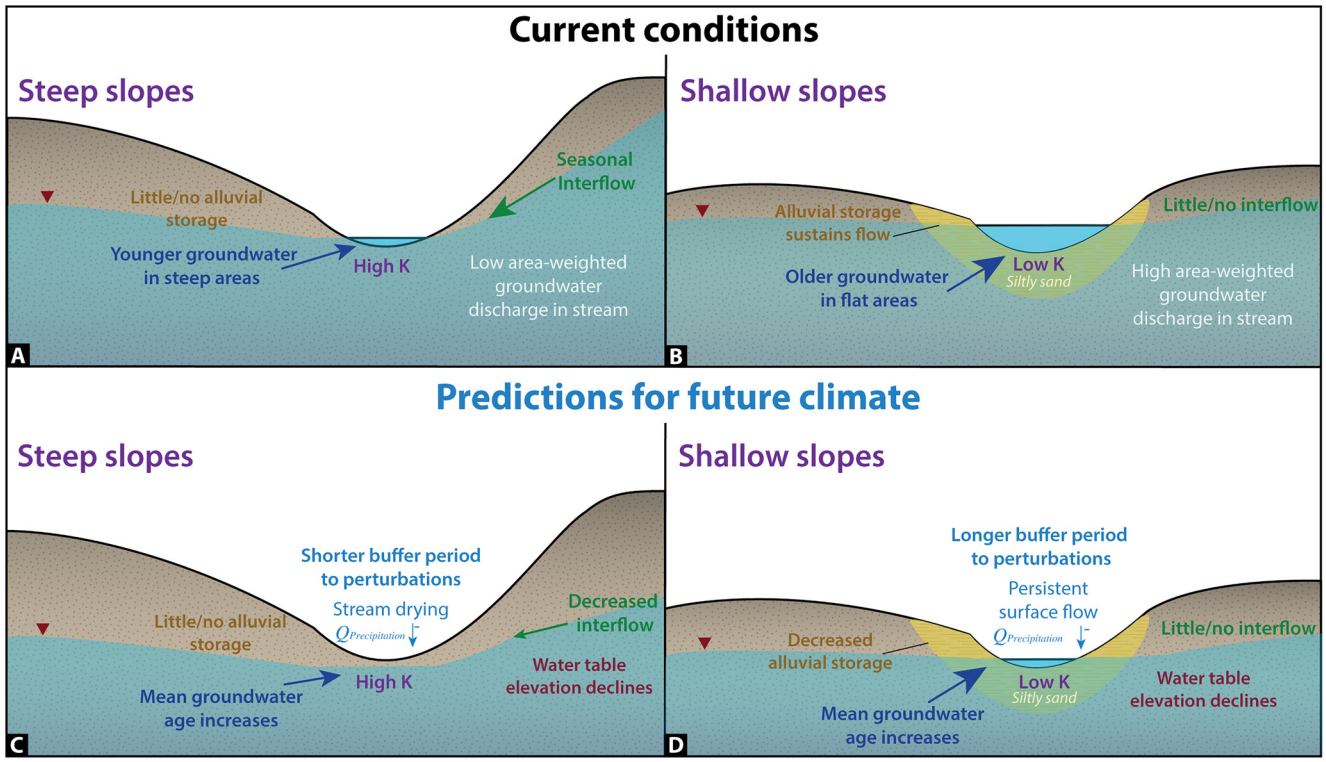

Figure 8. Conceptual figure showing hypothesized response to future decreased snow water equivalent and groundwater recharge in flat and steep scenarios in both a current and future setting. Text color is linked to different water sources and is consistent across subplots. In the top panels (a, b) we show current conditions at Manitou in a steep (panel (a)) and shallow slope (panel (b)) scenario. Currently, in steep areas streamflow is sourced by seasonal interflow and there is little to no alluvial storage. In these steep areas, there is a low upstream area-weighted groundwater discharge in the stream and groundwater age is young. In areas with shallower slopes, we observe little to no interflow or seasonal groundwater age shift. Groundwater age is relatively older and alluvial storage sustains high upstream area-weighted groundwater discharge to streamflow. The bottom two panels (c, d) show these two geomorphic settings in a future climate scenario. In steep areas (panel (c)) we hypothesize a groundwater table drop that causes stream drying. In areas with shallow slopes (panel (d)) we hypothesize that the groundwater table will still drop, but that alluvial storage can sustain short-term droughts and the older groundwater in these areas will enable a longer buffer period to perturbations.

groundwater remained relatively constant through time (Sites 1, 5, Figure S10 in Supporting Information S1). Site 6 was the only location that exhibited large changes in both groundwater age and the fraction of discharge from groundwater.

5. Discussion

We combined groundwater age estimates, end-member mixing results, and topographic analyses to assess how physical watershed properties impact streamflow resiliency in a small headwater catchment. We build on the established connection between topography and groundwater-surface water connection to illustrate how groundwater flow and storage vary in flat versus steep upstream contributing areas in current conditions (Figures 8a and 8b), and predicted response to changes in recharge (Figures 8c and 8d). Figure 8 serves as a graphical summary of the discussion section and illustrates many of the conclusions of the paper including how the hydraulic conductivity, changes in slope, role of interflow, presence of alluvial aquifers, and changes in groundwater age will impact future groundwater-surface water connection. The current conditions in the conceptual model are informed by the relative differences in groundwater-surface water connection observed at Manitou, as described below and in Section 5.2. In Section 5.3, we build off conditions observed today to predict how groundwater-surface water connection may vary in a future climate scenario.

5.1. Links Between Topography, Geology, Groundwater Age, and Stream Source

Groundwater residence time is a function of the entire flowpath, and conceptually where groundwater flowpaths are long, residence time will be older. However, we did not observe this trend as changes in groundwater residence

time did not follow any spatial pattern and groundwater was oldest in the upper catchment where upstream accumulation area is small. We instead show that the upstream area does not influence the residence time of groundwater contributing to streamflow. This connection corroborates findings from McGuire et al. (2005) who used oxygen isotopes to establish a similar conclusion that residence times are a function of watershed topography, rather than upstream area. Here, we build on this work to examine how changes in slope impact groundwater age and contribution to streamflow within a small headwater catchment.

In unconfined groundwater settings such as in the Manitou Experimental Forest, a steep topographic gradient may lead to a greater hydraulic gradient, driving hillslope groundwater to travel more quickly before contributing to streamflow and thus have a shorter residence time, as illustrated in Figure 8a. In topographically steep areas (Sites 2–6) we observed groundwater with a relatively young mean age, a large young fraction, and large seasonal increases in age. These factors point to a larger interflow contribution because of the temporally dynamic streamflow source. We attribute interflow and subsequent downslope drainage of hillslope regolith as the source of 1-year water for the young component and note that the Sites with the largest young fraction in June occur where slopes are steep. An existing hydrology study at Hotel Gulch shows that lateral groundwater sources from adjacent hillslopes (5–20 m from the stream) are a primary source to streamflow (Bush et al., 2023), corroborating the conclusion that hillslope topography is influencing groundwater in streamflow. On steeper slopes, shallow infiltration moves downslope more quickly and therefore may be less likely to infiltrate into the underlying bedrock, as shown by the green interflow arrow in Figure 8a. In the late summer and early fall, snowmelt-driven interflow may have largely drained from the system such that there is less contribution from very young water, explaining the large shifts in age at Sites 5 and 6 shown in Figure 6b. In these steep areas, we observed a lower area-weighted discharge from groundwater in stream flow (Figure 7c), indicating that more young, shallow flow is present in streamflow, relative to upstream locations (blue text in bottom right corner of Figure 8a).

In contrast, where upgradient slope is relatively flat, water moves more slowly, and old groundwater is stored before reaching the riparian zone (Figure 8b). In the flatter areas of Manitou, groundwater is routed from a constant source seasonally, rather than the flushing of recent infiltration. This constant groundwater source is evident in the temporally static groundwater specific conductivity patterns at Sites 7 and 8 (Figures 4g and 4h) where slopes are flat and groundwater is old relative to downstream locations. For example, in early August there was a large precipitation event that caused increases in discharge at all eight sites (Figure 2). There were subsequent decreases in groundwater specific conductivity at some locations, such as Sites 2 and 3 where slopes are steep and groundwater is young (Figures 3b and 3c), but specific conductivity stayed relatively constant in the upper watershed at Sites 7 and 8 where groundwater is older (Figures 3g and 3h). In addition, these flat areas had similar groundwater ages in both June and September (Figure 6a) and had the largest area-weighted groundwater contribution (Figure 7c). These two factors indicate relatively large and stable groundwater inputs, rather than distinct seasonal sources, such as the springtime interflow seen in steeper areas. The constant groundwater source in flat areas is illustrated in Figure 8b, where we show old groundwater with a high fraction of streamflow from groundwater in the stream, and little to no contribution from interflow.

Hillslope steepness is complicated by variable hillslope curvature patterns throughout Manitou. Others have investigated the role that curvature plays in groundwater flow and water table dynamics (Bachmair & Weiler, 2012) and found that the effects of convergent and divergent areas cancel their respective impacts on streamflow magnitude (Bogaart & Troch, 2006). Hillslope curvature is often simplified in groundwater flow models because of compounding heterogeneity in convex and concave sections within a single hillslope (Sabzevari & Noroozpour, 2014). Recent research has attempted to link groundwater transit time with variability in hillslope curvature and found a higher fraction of young flow in streams adjacent to simple convex hillslopes using numerical modeling (Xiao et al., 2021). These conclusions linking groundwater flow and hillslope curvature hold in low-frequency topography landscapes, but at Manitou we observe high-frequency, heterogeneous hillslope curvature where convex, concave, and linear segments can be found within a single hillslope, complicating our ability to isolate the role of curvature on groundwater age and its ability to contribute to streamflow. We note this as a limitation of this work but posit the potential to further improve prediction of future streamflow presence by pairing hillslope topography complexities through numerical modeling with empirical measurements of groundwater age and streamflow source, particularly as curvature has been shown to control the expansion and retraction of flowing streams (Prancevic & Kirchner, 2019).

In the flatter portions of the watershed, notably in the upper and lower watershed, channel and floodplain alluvium are mapped in the drainage bottom (Figure 1). We observed a connection between seasonal groundwater age increases and the presence of alluvial sediment. The three sites with little to no alluvial aquifer mapped adjacent

to the stream, Sites 4, 5, and 6 (Figure 1), have the largest seasonal shifts in age and magnitude of young fraction (Figures 6a and 6b, Figure S11 in Supporting Information S1). The small seasonal increase in age and young fraction at the other sites where alluvium is present (with the exception of the fault-influenced Site 1) suggest that in this headwater stream, alluvial aquifers store groundwater sourced from adjacent hillslopes and provide a mixing and storage compartment for interflow and bedrock discharge prior to discharging to streamflow, potentially providing a buffer to hydrologic perturbations. We illustrated this concept in Figures 8a and 8b by showing alluvial storage in flat areas (Figure 8b) and no alluvial storage in steeper areas (Figure 8a), consistent with observed channel and floodplain alluvium observed at Manitou. Site 1 is an exception here; we suggest that alluvial storage and interflow both contribute to young groundwater, but that fault-driven flow dominates surface water as indicated by discharge trends that are largely unresponsive to storm events (Figure 3b). Conclusions regarding the role of alluvial storage are novel as they incorporate age tracer data into existing hillslope hydrology literature.

In a short-term drought scenario, groundwater-sourced stream segments with adjacent alluvial aquifers may be more buffered to decreases in precipitation as compared to locations with no adjacent shallow alluvial aquifer. This conclusion is supported by seasonal age shifts where the largest seasonal increases in age coincided with locations where no alluvial fill is mapped, indicating a shifting groundwater source in response to recharge decreases. We note that Site 1 also exhibited a seasonal age increase and has a significant young component to flow, but we suggest that rather than mixing between interflow and bedrock in alluvial features, it is sourced by groundwater flow along the adjacent fault. The ability of alluvial storage to act as a buffer to recharge perturbations is also supported by a connection between low-flow area-weighted discharge and seasonal groundwater age increases. We saw that the minimum and maximum area-weighted discharge coincided with sites that had large and small changes in seasonal age on 25 September 2021. For example, Site 8 had the largest area-weighted discharge (0.91 L/s/km^2) and a small seasonal age shift (increase = 2 years) while Site 5 had the lowest area weighted discharge (0.09 L/s/km^2) and a large seasonal age shift (increase = 2 years), ignoring Site 2, which was dry at the time. We suggest that the alluvial fill in flat areas offers short-term storage that sustains a constant groundwater source during periods of limited recharge.

5.2. Connection Between Streambed Hydraulic Conductivity and Stream Discharge and Specific Conductivity

We observed a connection between streambed hydraulic conductivity, the area-weighted discharge from groundwater, and the mean age of discharging groundwater (Figures 7b and 7c), suggesting that shallow subsurface material at the streambed interface is impacting groundwater-surface water connection. In areas where older groundwater was present, there was also a relatively high fraction of precipitation in streamflow, such as at Sites 6–8 during the early season (Figures 5f–5h), compared to downstream Sites 1–4 that had a more constant fraction of discharge from streamflow throughout the season (Figures 5a–5d). We suggest that the constant fraction of discharge from streamflow is because low hydraulic conductivity soils prevented precipitation from quickly infiltrating the subsurface in the shallow-soil zone, particularly at Sites 7 and 8 where low hydraulic conductivity material surrounded the riparian zone. Instead, precipitation was largely routed to streamflow and potentially did not contribute to deeper groundwater. This is demonstrated, for example, at Site 7 where groundwater specific conductivity and groundwater level are stable through time (Figure 4g), despite flashy responses to precipitation events in the stream (Figure 3h). In addition, we also show that the fraction of discharge from groundwater had the largest increases groundwater age was temporally constant and hydraulic conductivity was low (Figure S10 in Supporting Information S1). This behavior is physical evidence of the preferential release of young streamflow because of subsurface heterogeneity as modeled in Berghuijs and Kirchner (2017) where groundwater with increasing age cannot sustain contributions to streamflow. In addition, the groundwater at Sites 7 and 8 was oldest and did not have a large young component during June, further indicating that recently infiltrated young groundwater is a primary source to shallow riparian groundwater. We illustrate this concept in Figure 8 by showing that old groundwater is located in locations with low hydraulic conductivity (Figure 8b) and that younger groundwater is found where hydraulic conductivity is high (Figure 8a).

We initially hypothesized that stream discharge and chemistry would be more seasonally constant in areas with old groundwater because it is more resistant to perturbations (Green et al., 2021). However, we observed that stream specific conductivity and discharge were not more stable where old groundwater was present near the stream, as indicated by poor correlation between mean age and the standard deviations of stream discharge

($R^2 = 0.07$, p-value = 0.53) and specific conductivity ($R^2 = 0.01$, p-value = 0.83) and instead conclude that streambed hydraulic conductivity is a primary control on groundwater in streamflow. We note that within the Manitou system groundwater is dominantly modern, and in larger-scale systems with groundwater of more widely varying age (up to hundreds to thousands of years old) the relation between age and stream specific conductivity may be significant at different scales.

Not surprisingly, we observed that streambed hydraulic conductivity plays a large role in the connection between streamflow and shallow groundwater, and thus can help inform where the groundwater-surface water connection will persist despite changes in recharge. Here we further corroborate existing knowledge of groundwater-surface water connection by incorporating groundwater age measurements with physical watershed properties. We note that hydraulic conductivity is heterogeneous through space and has been observed to vary through time (Rosenberry et al., 2021). For more robust conclusions, hydraulic conductivity should be measured at finer spatial and perhaps temporal scales to further improve characterization of controls on groundwater flow as we have identified it as a predictor of the ability of groundwater to contribute to streamflow, which is relevant to predicting stream permanence in future climate scenarios.

5.3. Implications for Stream Drying and Groundwater Age in Future Climate Scenarios

To predict how streams will respond to future climate change, hydrologists must be able to identify characteristics that allow a stream system to be more resilient to perturbations. Here, we build upon existing literature to contribute to the discussion about how headwater streams may respond to shifts in recharge patterns as a result of climate change by using a combination of groundwater age data, slope measurements, and streambed hydraulic conductivity as has been done in other studies, but incorporating groundwater age data as well. We present evidence that potential differences in the ability of groundwater to contribute to streamflow are driven by heterogeneity in physical properties such as slope and streambed hydraulic conductivity, as well as geologic features such as alluvial aquifers and faults. In Figures 8c and 8d we show a conceptual schematic illustrating how the groundwater-surface water connection may respond to changes in climate.

In a future where groundwater is the primary source of streamflow as recharge inputs decrease, we predict that streamflow is likely to persist despite decreases in snowpack in topographically flat areas where streambed hydraulic conductivity is low, as illustrated in Figure 8d. This conclusion is consistent with studies that have focused on relations between topography and stream-drying patterns and concluded that streams are most likely to dry in high-slope areas (Prancevic & Kirchner, 2019; Warix et al., 2021; Whiting & Godsey, 2016). However, these studies did not explore the role of hydraulic conductivity while trying to characterize how the shallow subsurface impacts the ability of groundwater to contribute to streamflow. In areas where streambed hydraulic conductivity is high and younger groundwater constitutes a high fraction of streamflow, we expect that stream drying will occur more frequently and for longer periods as decreases in hydrologic inputs cause groundwater tables to drop and high streambed hydraulic conductivity allows this drop to happen relatively quickly, as illustrated in Figure 8c. This prediction is supported by the stream drying that occurred at Site 2, which has the highest streambed hydraulic conductivity and a high fraction of discharge from groundwater in streamflow.

In Figures 8c and 8d, we show schematics illustrating predicted future changes in response to climate change in these two geomorphic settings. In both geomorphic settings we predict decreased water table elevation and increased mean groundwater age, relative to conditions today. In Figure 8c, where slopes are steep, we expect to see increases in stream drying as interflow contribution declines as a result of decreased infiltrating snow. We suggest that riparian groundwater at Manitou is partially sourced by interflow in steep areas. We observed the most dynamic shifts in groundwater age and lowest area-weighted groundwater discharge in steep areas where interflow contribute to streamflow. In a future climate scenario where precipitation decreases, sites primarily sourced by interflow will likely be among the first to dry as the precipitation available to supply interflow decreases (Figure 8c). In Figure 8d, we show flowing streams, despite decreases in water table elevation. Here, we suggest that where older, slow-moving groundwater as a result of low streambed hydraulic conductivity exists, old groundwater will act as a buffer to perturbations and enable groundwater supported streamflow to persist. Shallow alluvial aquifers throughout the watershed provide storage for this shallow old groundwater, as indicated by the seasonally constant groundwater age where alluvium is present. These shallow alluvial aquifers likely provide a buffer to hydrologic perturbations at short timescales, but have the potential to be depleted by an extended multi-year drought (Figure 8d).

The mean residence time of near-stream shallow groundwater at Manitou was 10–55 years; this timescale and potential lag in perturbations to streamflow is longer than most long-term hydrologic and geochemical data sets, acknowledging that groundwater celerity is often faster than its velocity (McDonnell & Beven, 2014). At the time of writing, the USGS hosts 72,485 hydrologic data sets with a mean data range of 14 years, with no constraints on continuous data collection. While many studies have focused on long-term changes in hydrologic and geochemical fluxes in headwater environments (Foks et al., 2018; Heil et al., 2022), the range of residence times we observe here and seen in other similar headwater environments (Georgek et al., 2017; Manning et al., 2012; Warix et al., 2021) exceeds the length of most long-term hydrologic and geochemical data sets. To observe how changes in climate are impacting how groundwater is stored and transported, the hydrologic community must continue to prioritize long-term data sets (Singha & Navarre-Sitchler, 2021), regardless of the age of groundwater.

We note a few limitations of these projections. Climate change is expected it impact multiple components of the Critical Zone, and we assume that vegetation uptake magnitudes and timing will not change, however it is currently unclear and beyond the scope of this paper how vegetation will respond to a changing climate. This study also only measured groundwater age tracers capable of dating modern groundwater (<70 years old). Premodern groundwater (>70 years old) has been observed in some mountainous bedrock catchments (Frisbee et al., 2013; Yager et al., 2013) and may discharge to streams (Bourke et al., 2014). Our samples therefore may contain some unaccounted-for premodern water, meaning our mean groundwater age estimates could be biased young due to our choice of age tracers (Mccallum et al., 2014). More data sets that incorporate a full suite of age tracers that can date both modern and premodern water are required to understand how climate change might affect the balance of modern and premodern water discharging to mountain streams.

6. Conclusions

We compared local slope, streambed hydraulic conductivity, and geology to mean groundwater age and groundwater contribution to streamflow at fine-spatial scales to identify topographic and subsurface characteristics that impact groundwater-surface water connection. While others have characterized controls on stream permanence, here we combine empirical groundwater age data with hydrograph separations to assess characteristics that enable stable surface flow today, and make predictions about future stream drying patterns.

We predict that stream drying is more probable where local slope and streambed hydraulic conductivity are high as we observed the most dynamic shifts in groundwater age and lowest area-weighted groundwater discharge in these steep areas. In relatively flatter areas, we predict more persistent streamflow despite recharge decreases as older groundwater residence times are more resistant to perturbations and shallow alluvial aquifers, in this system, provide some limited storage during drought periods. In this study, we demonstrate that watershed topography and hydraulic conductivity influence groundwater-surface water connection and may serve as predictors of future stream resilience in a headwater stream. Conclusions from this study likely vary at different watershed scales and serve as a starting point for improving quantification of how groundwater age and groundwater-surface water connection may change in the future.

Data Availability Statement

The timeseries, chemistry, and temperature profile data, as well as the reactive transport code used for evaluating changes in flow, end-member mixing analyses, and streambed hydraulic conductivity modeling in the study are available at Hydroshare at https://www.hydroshare.org/resource/46dc8efda0dd44a095592817d481fb1f.

Acknowledgments
We thank Samantha Motz, Sadie Jonson, Shradhanjli Ravikumar, and Luke Jacobsen for field assistance. In addition, we thank Holly Barnard and Sidney Bush for helpful discussions and precipitation data. Finally, we thank Steven Alton and Paula Fornwalt for Manitou Experimental Forest management. This work is supported by the National Science Foundation under Award EAR-2012730. Additional funding was provided by the Geological Society of America Graduate Student Research Grants program.

References

Abbott, B. W., Baranov, V., Mendoza-Lera, C., Nikolakopoulou, M., Harjung, A., Kolbe, T., et al. (2016). Using multi-tracer inference to move beyond single-catchment ecohydrology. *Earth-Science Reviews*, *160*, 19–42. https://doi.org/10.1016/j.earscirev.2016.06.014

Acuña, V., Hunter, M., & Ruhí, A. (2017). Managing temporary streams and rivers as unique rather than second-class ecosystems. *Biological Conservation*, *211*, 12–19. https://doi.org/10.1016/j.biocon.2016.12.025

Aeschbach-Hertig, W., Peeters, F., Beyerle, U., & Kipfer, R. (2000). Paleotemperature reconstruction from noble gases in groundwater accounting for equilibration with entrapped air. *Nature*, *405*(June), 1040–1044. https://doi.org/10.1038/35016542

Althaus, R., Klump, S., Onnis, A., Kipfer, R., Purtschert, R., Stauffer, F., & Kinzelbach, W. (2009). Noble gas tracers for characterisation of flow dynamics and origin of groundwater: A case study in Switzerland. *Journal of Hydrology*, *370*(1–4), 64–72. https://doi.org/10.1016/j.jhydrol.2009.02.053

Bachmair, S., & Weiler, M. (2012). Hillslope characteristics as controls of subsurface flow variability. *Hydrology and Earth System Sciences*, *16*(10), 3699–3715. https://doi.org/10.5194/hess-16-3699-2012

Berghuijs, W. R., & Kirchner, J. W. (2017). The relationship between contrasting ages of groundwater and streamflow. *Geophysical Research Letters*, *44*(17), 8925–8935. https://doi.org/10.1002/2017GL074962

Blair, R. W. (1976). Weathering and geomorphology of the Pikes peak granite in the southern Rampart range, Colorado. In *Professional contributions of Colorado School of Mines: Studies in Colorado field geology* (Vol. 8, pp. 68–72).

Blöschl, G., Bierkens, M. F. P., Chambel, A., Cudennec, C., Destouni, G., Fiori, A., et al. (2019). Twenty-three unsolved problems in hydrology (UPH)–a community perspective. *Hydrological Sciences Journal*, *64*(10), 1141–1158. https://doi.org/10.1080/02626667.2019.1620507

Bockgård, N., Rodhe, A., & Olsson, K. A. (2004). Accuracy of CFC groundwater dating in a crystalline bedrock aquifer: Data from a site in southern Sweden. *Hydrogeology Journal*, *12*(2), 171–183. https://doi.org/10.1007/s10040-004-0319-3

Bogaart, P. W., & Troch, P. A. (2006). Curvature distribution within hillslopes and catchments and its effect on the hydrological response. *Hydrology and Earth System Sciences*, *10*(6), 925–936. https://doi.org/10.5194/hess-10-925-2006

Bourke, S. A., Harrington, G. A., Cook, P. G., Post, V. E., & Dogramaci, S. (2014). Carbon-14 in streams as a tracer of discharging groundwater. *Journal of Hydrology*, *519*(PA), 117–130. https://doi.org/10.1016/j.jhydrol.2014.06.056

Brunner, P., Cook, P. G., & Simmons, C. T. (2009). Hydrogeologic controls on disconnection between surface water and groundwater. *Water Resources Research*, *45*(1), 1–13. https://doi.org/10.1029/2008WR006953

Busenberg, E., & Plummer, N. (1992). Use of chlorofluorocarbons (CCl3F and CCl2F2) as hydrologic tracers and age-dating tools: The alluvium and terrace system of Central Oklahoma. *Water Resources*, *28*(9), 2257–2283. https://doi.org/10.1029/92wr01263

Busenberg, E., Weeks, E., Plummer, N., & Bartholomay, R. (1993). *Age dating ground water by use of chlorofluorocarbons (CCl3F and CCl2F2), and distribution of chlorofluorocarbons in the unsaturated zone, snake river plain aquifer, Idaho national engineering laboratory, Idaho*. Ground Water (p. 52). US Department of Interior, US Geological Survey.

Bush, S. A., Birch, A. L., Warix, S. R., Sullivan, P. L., Gooseff, M. N., Mcknight, D. M., & Barnard, H. R. (2023). Dominant source areas shift seasonally from longitudinal to lateral contributions in a montane headwater stream. *Journal of Hydrology*, *617*, 129134. https://doi.org/10.1016/j.jhydrol.2023.129134

Carroll, R. W. H., Deems, J. S., Niswonger, R., Schumer, R., & Williams, K. H. (2019). The importance of interflow to groundwater recharge in a snowmelt-dominated headwater basin. *Geophysical Research Letters*, *46*(11), 5899–5908. https://doi.org/10.1029/2019GL082447

Carroll, R. W. H., Manning, A. H., Niswonger, R., Marchetti, D., & Williams, K. H. (2020). Baseflow age distributions and depth of active groundwater flow in a snow-dominated mountain headwater basin. *Water Resources Research*, *56*(12), 1–19. https://doi.org/10.1029/2020WR028161

Christensen, L., Tague, C., & Baron, J. S. (2008). Spatial patterns of simulated transpiration response to climate variability in a snow dominated mountain ecosystem. *Hydrological Processes*, *22*(18), 3576–3588. https://doi.org/10.1002/hyp

Cook, P. G., & Böhlke, J.-K. (2000). Determining timescales for groundwater flow and solute transportnin. In *Environmental tracers in subsurface hydrology* (pp. 1–30). Kluwer Academic Publishers.

Cuthbert, M. O., Gleeson, T., Moosdorf, N., Befus, K. M., Schneider, A., Hartmann, J., & Lehner, B. (2019). Global patterns and dynamics of climate–groundwater interactions. *Nature Climate Change*, *9*(2), 137–141. https://doi.org/10.1038/s41558-018-0386-4

Datry, T., Larned, S. T., & Tockner, K. (2014). Intermittent rivers: A challenge for freshwater ecology. *BioScience*, *64*(3), 229–235. https://doi.org/10.1093/biosci/bit027

Dohman, J. M., Godsey, S. E., & Hale, R. L. (2021). Three-dimensional subsurface flow path controls on flow permanence. *Water Resources Research*, *57*(10), 1–18. https://doi.org/10.1029/2020WR028270

Earman, S., & Dettinger, M. (2011). Potential impacts of climate change on groundwater resources - A global review. *Journal of Water and Climate Change*, *2*(4), 213–229. https://doi.org/10.2166/wcc.2011.034

Foks, S. S., Stets, E. G., Singha, K., & Clow, D. W. (2018). Influence of climate on alpine stream chemistry and water sources. *Hydrological Processes*, *32*(13), 1993–2008. https://doi.org/10.1002/hyp.13124

Fovet, O., Belemtougri, A., Boithias, L., Braud, I., Charlier, J. B., Cottet, M., et al. (2021). Intermittent rivers and ephemeral streams: Perspectives for critical zone science and research on socio-ecosystems. *Wiley Interdisciplinary Reviews: Water*, *8*(4), 1–33. https://doi.org/10.1002/wat2.1523

Frisbee, M. D., Wilson, J. L., Gomez-Velez, J. D., Phillips, F. M., & Campbell, A. R. (2013). Are we missing the tail (and the tale) of residence time distributions in watersheds. *Geophysical Research Letters*, *40*(17), 4633–4637. https://doi.org/10.1002/grl.50895

Gardner, W. P., Jensco, K., H Hoylman, Z., Livesay, R., & P Maneta, M. (2020). A numerical investigation of bedrock groundwater recharge and exfiltration on soil mantled hillslopes. *Hydrological Processes*, *34*(15), 3311–3330. https://doi.org/10.1002/hyp.13799

Georgek, J. L., Kip Solomon, D., Heilweil, V. M., & Miller, M. P. (2017). Using tracer-derived groundwater transit times to assess storage within a high-elevation watershed of the upper Colorado River Basin, USA. *Hydrogeology Journal*, *26*(2), 467–480. https://doi.org/10.1007/s10040-017-1655-4

Gleeson, T., & Manning, A. H. (2008). Regional groundwater flow in mountainous terrain: Three-dimensional simulations of topographic and hydrogeologic controls. *Water Resources Research*, *44*(10), 1–16. https://doi.org/10.1029/2008WR006848

Green, C. T., Ransom, K. M., Nolan, B. T., Liao, L., & Harter, T. (2021). Machine learning predictions of mean ages of shallow well samples in the Great Lakes Basin, USA. *Journal of Hydrology*, *603*(PB), 126908. https://doi.org/10.1016/j.jhydrol.2021.126908

Hale, C. V., & McDonnell, J. J. (2016). Effect of bedrock permeability on stream base flow mean transit time scaling relations: 1. A multiscale catchment intercomparison. *Water Resources Research*, *55*(2), 1358–1374. https://doi.org/10.1111/j.1752-1688.1969.tb04897.x

Heil, E., Warix, S., Singha, K., & Navarre-Sitchler, A. (2022). Decadal trends in solute concentrations, mass flux, and discharge reveal variable hydrologic and geochemical response to climate change in two alpine watersheds. *Applied Geochemistry*, *144*, 105402. https://doi.org/10.1016/j.apgeochem.2022.105402

Hood, J. L., Roy, J. W., & Hayashi, M. (2006). Importance of groundwater in the water balance of an alpine headwater lake. *Geophysical Research Letters*, *33*(13), 1–5. https://doi.org/10.1029/2006GL026611

Jurgens, B. C. (2018). *Data for Tritium deposition in precipitation in the United States, 1953 - 2012*: U.S. Geological Survey data release. https://doi.org/10.5066/P92CEFXN

Jurgens, B. C., Böhlke, J. K., & Eberts, S. M. (2012). TracerLPM (Version 1): An Excel® workbook for interpreting groundwater age distributions from environmental tracer data. U.S. Geological Survey Techniques and Methods Report 4-F3 (p. 60).

Jurgens, B. C., Faulkner, K., Mcmahon, P. B., Hunt, A. G., Casile, G., Young, M. B., & Belitz, K. (2022). Over a third of groundwater in USA public-supply aquifers is Anthropocene-age and susceptible to surface contamination. *Communications Earth & Environment*, *3*(153), 1–9. https://doi.org/10.1038/s43247-022-00473-y

Kasahara, T., & Wondzell, S. M. (2003). Geomorphic controls on hyporheic exchange flow in mountain streams. *Water Resources Research*, *39*(1), SBH3-1–SBH3-14. https://doi.org/10.1029/2002wr001386

Katsuyama, M., Tani, M., & Nishimoto, S. (2010). Connection between streamwater mean residence time and bedrock groundwater recharge/discharge dynamics in weathered granite catchments. *Hydrological Processes*, *24*(16), 2287–2299. https://doi.org/10.1002/hyp.7741

Klos, Z. P., Link, T. E., & Abatzoglou, J. T. (2014). Extent of the rain-snow transition zone in the western U.S. under historic and projected climate. *Geophysical Prospecting*, 6413–6419. https://doi.org/10.1002/2014GL061184.Received

Manning, A. H. (2011). Mountain-block recharge, present and past, in the eastern Española Basin, New Mexico, USA. *Hydrogeology Journal*, *19*(2), 379–397. https://doi.org/10.1007/s10040-010-0696-8

Manning, A. H., Ball, L. B., Wanty, R. B., & Williams, K. H. (2021). Direct observation of the depth of active groundwater circulation in an alpine watershed. *Water Resources Research*, *57*(2), e2020WR028548. https://doi.org/10.1029/2020WR028548

Manning, A. H., Clark, J. F., Diaz, S. H., Rademacher, L. K., Earman, S., & Niel Plummer, L. (2012). Evolution of groundwater age in a mountain watershed over a period of thirteen years. *Journal of Hydrology*, *460*(461), 13–28. https://doi.org/10.1016/j.jhydrol.2012.06.030

Manning, A. H., Runkel, R. L., Morrison, J. M., Wanty, R. B., & Walton-Day, K. (2022). Incorporating streambank wells in stream mass loading studies to more effectively identify sources of solutes in stream water. *Applied Geochemistry*, *145*(August), 105425. https://doi.org/10.1016/j.apgeochem.2022.105425

Marçais, J., Derry, L. A., Guillaumot, L., Aquilina, L., & Dreuzy, J. (2022). Dynamic contributions of stratified groundwater to streams controls seasonal variations of streamwater transit times. *Water Resources Research*, *58*(3), 1–22. https://doi.org/10.1029/2021wr029659

Mccallum, J. L., Cook, P. G., Simmons, C. T., & Werner, A. D. (2014). Bias of apparent tracer ages in heterogeneous environments. *Groundwater*, *52*(2), 239–250. https://doi.org/10.1111/gwat.12052

McDonnell, J. J., & Beven, K. (2014). Debates - the future of hydrological sciences: A (common) path forward? A call to action aimed at understanding velocities, celerities and residence time distributions of the headwater hydrograph. *Water Resources Research*, *50*(6), 5342–5350. https://doi.org/10.1002/2013WR015141

McGuire, K. J., & McDonnell, J. J. (2006). A review and evaluation of catchment transit time modeling. *Journal of Hydrology*, *330*(3–4), 543–563. https://doi.org/10.1016/j.jhydrol.2006.04.020

McGuire, K. J., McDonnell, J. J., Weiler, M., Kendall, C., McGlynn, B. L., Welker, J. M., & Seibert, J. (2005). The role of topography on catchment-scale water residence time. *Water Resources Research*, *41*(5), 1–14. https://doi.org/10.1029/2004WR003657

Meixner, T., Manning, A. H., Stonestrom, D. A., Allen, D. M., Ajami, H., Blasch, K. W., et al. (2016). Implications of projected climate change for groundwater recharge in the western United States. *Journal of Hydrology*, *534*, 124–138. https://doi.org/10.1016/j.jhydrol.2015.12.027

Meyers, Z. P., Frisbee, M. D., Rademacher, L. K., & Stewart-Maddox, N. S. (2021). Old groundwater buffers the effects of a major drought in groundwater-dependent ecosystems of the eastern Sierra Nevada (CA). *Environmental Research Letters*, *16*(4), 044044. https://doi.org/10.1088/1748-9326/abde5f

Miller, M. P., Susong, D. D., Shope, C. L., Heilweil, V. M., & Stolp, B. J. (2014). Continuous estimation of baseflow in snowmelt-dominated streams and rivers in the upper Colorado River Basin: A chemical hydrograph separation approach. *Water Resources Research*, *50*(8), 6986–6999. https://doi.org/10.1002/2013WR014939

Moidu, H., Obedzinski, M., Carlson, S. M., & Grantham, T. E. (2021). Spatial patterns and sensitivity of intermittent stream drying to climate variability. *Water Resources Research*, *57*(11), 1–14. https://doi.org/10.1029/2021WR030314

Moore, R. (1992). *Soil survey of Pike national forest, Eastern Park, Colorado, parts of Douglas, El Paso, Jefferson, and Teller counties*. USDA Forest Service and Soil Conservation Service.

Moore, R. D. D. (2005). Slug Injection using salt in solution. *Streamline, Watershed Management Bulletin*, *8*(2), 1–6. https://doi.org/10.1592/phco.23.9.1S.32890

Musselman, K. N., Addor, N., Vano, J. A., & Molotch, N. P. (2021). Winter melt trends portend widespread declines in snow water resources. *Nature Climate Change*, *11*(5), 418–424. https://doi.org/10.1038/s41558-021-01014-9

National Atmospheric Deposition Program. (2022). *National atmospheric deposition program (NRSP-3)* (Vol. 465). NADP Program Office, Wisconsin State Laboratory of Hygiene.

Pinder, G. F., & Jones, J. F. (1969). Determination of the ground-water component of peak discharge from the chemistry of total runoff. *Water Resources Research*, *5*(2), 438–445. https://doi.org/10.1029/wr005i002p00438

Plummer, L. N., & Busenberg, E. (2000). Chlorofluorocarbons. In P. G. Cook & A. L. Herczeg (Eds.), *Environmental tracers in subsurface hydrology* (pp. 441–478). Kluwer Academic Publishers.

Popp, A. L., Pardo-Álvarez, Á., Schilling, O. S., Scheidegger, A., Musy, S., Peel, M., et al. (2021). A framework for untangling transient groundwater mixing and travel times. *Water Resources Research*, *57*(4), 1–16. https://doi.org/10.1029/2020WR028362

Prancevic, J. P., & Kirchner, J. W. (2019). Topographic controls on the extension and retraction of flowing streams. *Geophysical Research Letters*, *46*(4), 2084–2092. https://doi.org/10.1029/2018GL081799

Quichimbo, E. A., Singer, M. B., & Cuthbert, M. O. (2020). Characterising groundwater–surface water interactions in idealised ephemeral stream systems. *Hydrological Processes*, *34*(18), 3792–3806. https://doi.org/10.1002/hyp.13847

Rademacher, L. K., Clark, J. F., Clow, D. W., & Hudson, G. B. (2005). Old groundwater influence on stream hydrochemistry and catchment response times in a small Sierra Nevada catchment: Sagehen Creek, California. *Water Resources Research*, *41*(2), 1–10. https://doi.org/10.1029/2003WR002805

Reynolds, L. V., Shafroth, P. B., & LeRoy Poff, N. (2015). Modeled intermittency risk for small streams in the Upper Colorado River Basin under climate change. *Journal of Hydrology*, *523*, 768–780. https://doi.org/10.1016/j.jhydrol.2015.02.025

Rosenberry, D. O., Engesgaard, P., & Hatch, C. (2021). Hydraulic conductivity can no longer be considered a fixed property when quantifying flow between groundwater and surface water. *Hydrological Processes*, *35*(6), 1–7. https://doi.org/10.1002/hyp.14226

Rossi, M. W., Anderson, S. P., Anderson, R. S., & Tucker, G. E. (2022). *Bedrock exposure, canopy density, and runoff generation in the Rampart Range, CO 2018*. National Center for Airborne Laser Mapping (NCALM). https://doi.org/10.5069/G9CV4FXZ

Sabzevari, T., & Noroozpour, S. (2014). Effects of hillslope geometry on surface and subsurface flows. *Hydrogeology Journal*, *22*(7), 1593–1604. https://doi.org/10.1007/s10040-014-1149-6

Saraiva Okello, A. M. L., Uhlenbrook, S., Jewitt, G. P. W., Masih, I., Riddell, E. S., & Van der Zaag, P. (2018). Hydrograph separation using tracers and digital filters to quantify runoff components in a semi-arid mesoscale catchment. *Hydrological Processes*, *32*(10), 1334–1350. https://doi.org/10.1002/hyp.11491

Sauquet, E., Beaufort, A., Sarremejane, R., & Thirel, G. (2021). Predicting flow intermittence in France under climate change. *Hydrological Sciences Journal*, *66*(14), 2046–2059. https://doi.org/10.1080/02626667.2021.1963444

Sebol, L. A., Robertson, W. D., Busenberg, E., Plummer, L. N., Ryan, M. C., & Schiff, S. L. (2007). Evidence of CFC degradation in groundwater under pyrite-oxidizing conditions. *Journal of Hydrology*, *347*(1–2), 1–12. https://doi.org/10.1016/j.jhydrol.2007.08.009

Segura, C. (2021). Snow drought reduces water transit times in headwater streams. *Hydrological Processes*, *35*(12), 1–17. https://doi.org/10.1002/hyp.14437

Seltzer, A. M., Ng, J., Aeschbach, W., Kipfer, R., Kulongoski, J. T., Severinghaus, J. P., & Stute, M. (2021). Widespread six degrees celsius cooling on land during the last glacial maximum. *Nature*, *593*(7858), 228–232. https://doi.org/10.1038/s41586-021-03467-6

Shanafield, M., Bourke, S. A., Zimmer, M. A., & Costigan, K. H. (2021). An overview of the hydrology of non-perennial rivers and streams. *Wiley Interdisciplinary Reviews: Water*, *8*(2), e1504. https://doi.org/10.1002/wat2.1504

Siirila-Woodburn, E. R., Rhoades, A. M., Hatchett, B. J., Huning, L. S., Szinai, J., Tague, C., et al. (2021). A low-to-no snow future and its impacts on water resources in the western United States. *Nature Reviews Earth & Environment*, *2*(11), 800–819. https://doi.org/10.1038/s43017-021-00219-y

Singha, K., & Navarre-Sitchler, A. (2021). The importance of groundwater in critical zone science. *Groundwater*, *60*, 1–8. https://doi.org/10.1111/gwat.13143

Sklash, M. G., Farvolden, R. N., & Fritz, P. (1976). A conceptual model of watershed response to rainfall, developed through the use of oxygen-18 as a natural tracer. *Canadian Journal of Earth Sciences*, *13*(5), 715. https://doi.org/10.1139/e76-076

Soil Survey Staff, Natural Resources Conservation Service, & United States Department of Agriculture. (2023). Web soil survey. Retrieved from http://websoilsurvey.sc.egov.usda.gov/

Sprenger, M., Stumpp, C., Weiler, M., Aeschbach, W., Allen, S. T., Benettin, P., et al. (2019). The demographics of water: A review of water ages in the critical zone. *Reviews of Geophysics*, *57*(3), 800–834. https://doi.org/10.1029/2018RG000633

Sprenger, M., Tetzlaff, D., Buttle, J., Laudon, H., & Soulsby, C. (2018). Water ages in the critical zone of long-term experimental sites in northern latitudes. *Hydrology and Earth System Sciences*, *22*(7), 3965–3981. https://doi.org/10.5194/hess-22-3965-2018

Stephens, C. M., Marshall, L. A., Johnson, F. M., Ajami, H., Lin, L., & Band, L. E. (2022). Spatial variation in catchment response to climate change depends on lateral moisture transport and nutrient dynamics. *Water Resources Research*, *58*(10), 1–20. https://doi.org/10.1029/2021WR030577

Stubbington, R., England, J., Wood, P. J., & Sefton, C. E. M. (2017). Temporary streams in temperate zones: Recognizing, monitoring and restoring transitional aquatic-terrestrial ecosystems. *Wiley Interdisciplinary Reviews: Water*, *4*(4), 1–17. https://doi.org/10.1002/WAT2.1223

Stute, M., & Schlosser, P. (2000). Atmospheric noble gases. In *Environmental tracers in subsurface hydrology* (pp. 349–377). Springer US.

Suckow, A., Araguás, L., & Aggarwall, P. K. (Eds.) (2013). Isotope methods, *Isotope methods for dating old groundwater*. International Atomic Energy Agency. https://doi.org/10.1080/10406029809379327

Temple, J., Madole, R., Keller, J. W., & Martin, D. (2007). Geologic map of the Mount Deception quadrangle, Teller and El Paso counties, Colorado. Colorado Geological Survey, Open-File Report OF-07-07.

Tripathi, M., Yadav, P. K., Chahar, B. R., & Dietrich, P. (2021). A review on groundwater–surface water interaction highlighting the significance of streambed and aquifer properties on the exchanging flux. *Environmental Earth Sciences*, *80*(17), 1–16. https://doi.org/10.1007/s12665-021-09897-9

Uhlenbrook, S., Frey, M., Leibundgut, C., & Maloszewski, P. (2002). Hydrograph separations in a mesoscale mountainous basin at event and seasonal timescales. *Water Resources Research*, *38*(6), 31-1–31-14. https://doi.org/10.1029/2001wr000938

University of Miami Tritium Laboratory. (2021). *Advise on Tritium sampling*. University of Miami Tritium Laboratory. Retrieved from https://tritium.rsmas.miami.edu/analytical-services/advice-on-sampling/index.html

Urióstegui, S. H., Bibby, R. K., Esser, B. K., & Clark, J. F. (2017). Quantifying annual groundwater recharge and storage in the central Sierra Nevada using naturally occurring 35S. *Hydrological Processes*, *31*(6), 1382–1397. https://doi.org/10.1002/hyp.11112

USGS. (2021). *U.S. Geological Survey groundwater age dating laboratory* (pp. 5–9). U.S. Geological Survey. Retrieved from http://water.usgs.gov/lab/

Voytek, E. B., Drenkelfuss, A., Day-Lewis, F. D., Healy, R., Lane, J. W., & Werkema, D. (2014). 1DTempPro: Analyzing temperature profiles for groundwater/surface-water exchange. *Groundwater*, *52*(2), 298–302. https://doi.org/10.1111/gwat.12051

Wanty, R. B., Folger, P. F., Frishman, D., Briggs, P. H., Day, W. C., & Poeter, E. (1992). *Weathering of Pikes peak granite: Field, experimental, and modelling observations*. Water-Rock Interaction.

Warix, S. R., Godsey, S. E., Lohse, K. A., & Hale, R. L. (2021). Influence of groundwater and topography on stream drying in semi-arid headwater streams. *Hydrological Processes*, *35*(5), 1–18. https://doi.org/10.1002/hyp.14185

Weinstein, L. H. (1977). Fluoride and plant life. *Journal of Occupational Medicine*, *19*(1), 49–78. https://doi.org/10.1097/00043764-197701000-00005

White, A., Ma, L., Moravec, B., Chorover, J., & McIntosh, J. (2021). U-series and Sr isotopes as tracers of mineral weathering and water routing from the deep Critical Zone to streamflow in a high-elevation volcanic catchment. *Chemical Geology*, *570*(March), 120156. https://doi.org/10.1016/j.chemgeo.2021.120156

Whiting, J. A., & Godsey, S. E. (2016). Discontinuous headwater stream networks with stable flowheads, Salmon River basin, Idaho. *Hydrological Processes*, *30*(13), 2305–2316. https://doi.org/10.1002/hyp.10790

Winter, T. C. (2001). The concept of hydrologic landscapes. *Journal of the American Water Resources Association*, *37*(2), 335–349. https://doi.org/10.1111/j.1752-1688.2001.tb00973.x

Winter, T. C., Harvey, J. W., Franke, O. L., & William, A. M. (1998). *Groundwater and surface water: A single resource* (Vol. 1139). U.S. Geological Survey Circular.

Wohl, E. (2017). The significance of small streams. *Frontiers of Earth Science*, *11*(3), 447–456. https://doi.org/10.1007/s11707-017-0647-y

Xiao, D., Brantley, S. L., & Li, L. (2021). Vertical connectivity regulates water transit time and chemical weathering at the hillslope scale. *Water Resources Research*, *57*(8), 1–21. https://doi.org/10.1029/2020WR029207

Yager, R. M., Plummer, L. N., Kauffman, L. J., Doctor, D. H., Nelms, D. L., & Schlosser, P. (2013). Comparaison de la distribution statistique de l'âge des eaux estimée avec des traceurs environnementaux, en utilisant des modèles numériques de mélange binaire et le modèle numérique d'un karst fracturé et plissé: Vallée de Shenandoah, Virginie, et Ouest. *Hydrogeology Journal*, *21*(6), 1193–1217. https://doi.org/10.1007/s10040-013-0997-9

Zapata-Rios, X., Brooks, P. D., Troch, P. A., McIntosh, J., & Rasmussen, C. (2016). Influence of climate variability on water partitioning and effective energy and mass transfer in a semi-arid critical zone. *Hydrology and Earth System Sciences*, *20*(3), 1103–1115. https://doi.org/10.5194/hess-20-1103-2016

Zaremehrjardy, M., Victor, J., Park, S., Smerdon, B., Alessi, D. S., & Faramarzi, M. (2022). Assessment of snowmelt and groundwater-surface water dynamics in mountains, foothills, and plains regions in northern latitudes. *Journal of Hydrology*, *606*(August 2021), 127449. https://doi.org/10.1016/j.jhydrol.2022.127449

References From the Supporting Information

Godinho, J. R. A., Piazolo, S., & Evins, L. Z. (2012). Effect of surface orientation on dissolution rates and topography of CaF 2. *Geochimica et Cosmochimica Acta*, *86*, 392–403. https://doi.org/10.1016/j.gca.2012.02.032